ACS OMEGA

Open Access

http://pubs.acs.org/journal/acsodf

Article

Normal Mode Analysis Elicits Conformational Shifts in Proteins at Both Proximal and Distal Regions to the Phosphosite Stemming from Single-Site Phosphorylation

Seemadri Subhadarshini, Himani Tandon, Narayanaswamy Srinivasan, and Ramanathan Sowdhamini*

Cite This: *ACS Omega* 2024, 9, 24520−24537

Read Online

ACCESS | Metrics & More | Article Recommendations | Supporting Information

ABSTRACT: Phosphorylation, a fundamental biochemical switch, intricately regulates protein function and signaling pathways. Our study employs extensive computational structural analyses on a curated data set of phosphorylated and unphosphorylated protein pairs to explore the multifaceted impact of phosphorylation on protein conformation. Using normal mode analysis (NMA), we investigated changes in protein flexibility post-phosphorylation, highlighting an enhanced level of structural dynamism. Our findings reveal that phosphorylation induces not only local changes at the phosphorylation site but also extensive alterations in distant regions, showcasing its far-reaching influence on protein structure-dynamics. Through in-depth case studies on polyubiquitin B and glycogen synthase kinase-3 beta, we elucidate how phosphorylation at distinct sites leads to variable structural and dynamic modifications, potentially dictating functional outcomes. While phosphorylation largely preserves the residue motion correlation, it significantly disrupts low-frequency global modes, presenting a dualistic impact on protein dynamics. We also explored alterations in the total accessible surface area (ASA), emphasizing region-specific changes around phosphorylation sites. This study sheds light on phosphorylation-induced conformational changes, dynamic modulation, and surface accessibility alterations, leveraging an integrated computational approach with RMSD, NMA, and ASA, thereby contributing to a comprehensive understanding of cellular regulation and suggesting promising avenues for therapeutic interventions.

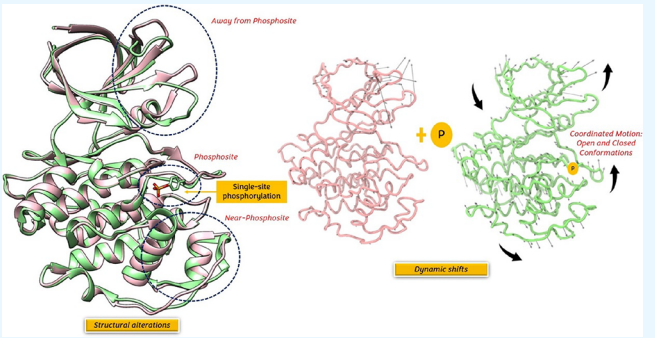

INTRODUCTION

Phosphorylation is a prevalent and crucial post-translational modification (PTM) that plays a fundamental role in regulating protein function and cellular signaling. It is involved in a wide range of cellular processes, including cell cycle regulation, metabolism, signal transduction, and gene expression.[1,2] In eukaryotes, serine, threonine, and tyrosine residues are frequently phosphorylated. Among these, serine is the most predominant followed by threonine and then tyrosine.[3] On the other hand, in prokaryotes, histidine residues serve as the primary phosphorylation sites. This enzymatic addition of a phosphate group, facilitated by protein kinases, acts as a molecular switch, modulating protein activity, localization, and interactions.[4] Phosphorylation is a highly regulated process that enables cells to rapidly respond to external stimuli by activating or deactivating specific proteins or signaling cascades.[5] It exerts its regulatory effects through various mechanisms, including inducing conformational changes that expose or hide functional domains, creating binding sites for other proteins, or disrupting existing interactions, influencing subcellular localization, and regulating enzymatic activity. These phosphorylation events orchestrate intricate cellular signaling networks,[6,7] enabling cells to adapt and respond to changing environmental conditions.

Numerous studies have demonstrated that when proteins interact with effector molecules, such as small molecules, proteins, DNA/RNA, mutations, or other post-translational modifications,[8] they undergo structural modifications, changes in dynamics and flexibility, and alterations in surface accessibility. These changes can occur not only at the binding site but also in the distal regions. The effector molecule can induce significant conformational alterations in the protein, either locally or globally, or cause subtle shifts in the equilibrium between different conformations.[8,9] The present study focuses on elucidating the intricacies of phosphorylation-induced structure-dynamics-accessibility alterations. By focusing on this post-translational modification, our research aims to

Received: January 16, 2024
Revised: April 29, 2024
Accepted: May 13, 2024
Published: May 30, 2024

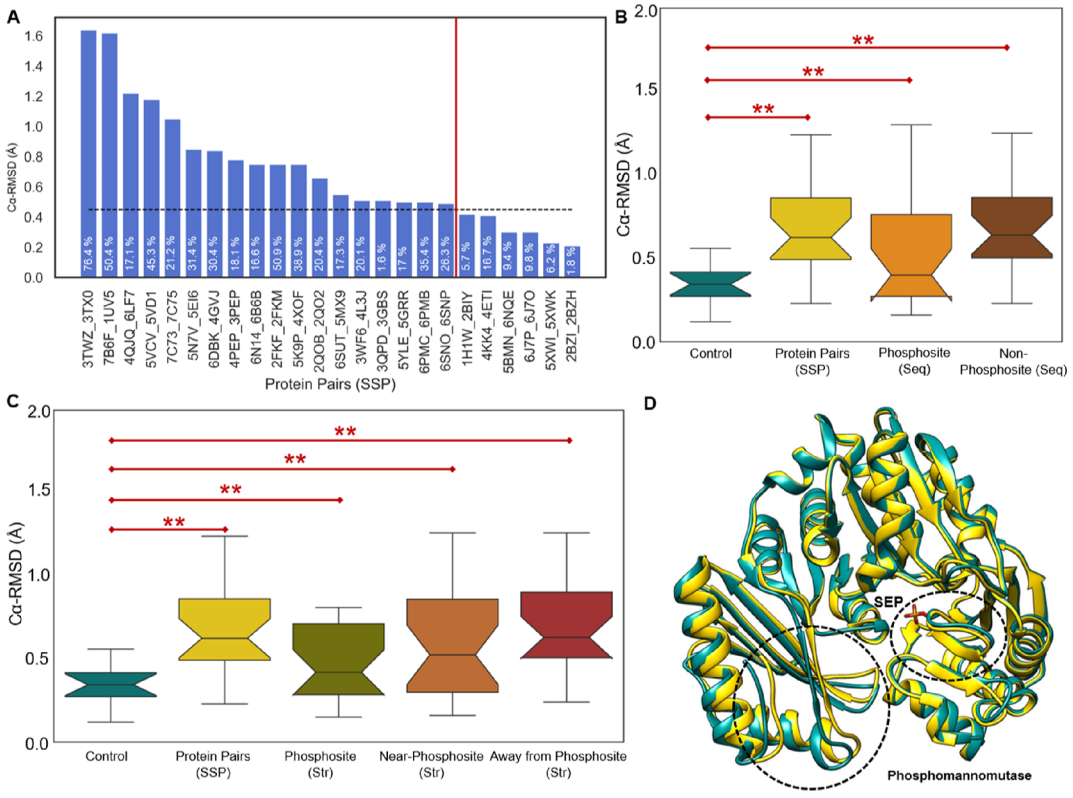

Figure 1. Comparative structural analyses of the SSP data set. (A) Bar plot depicting Cα-RMSD for protein pairs. A higher RMSD indicates a greater structural disparity between phosphorylated and unphosphorylated forms. The black line denotes the cutoff derived from the control data set, with bars to the left of the red line signifying significant structural changes and those to the right as not significant. The percentage of residues with Cα-deviation greater than that of control, for each protein pair in the SSP data set, is indicated. (B) Box plots showing the distribution of Cα-RMSD (Å) for the control data set, protein pairs in the SSP data set, phosphosite (Seq), and non-phosphosite (Seq). (C) Box plots displaying the distribution of Cα-RMSD (Å) for the control data set, protein pairs in the SSP data set, phosphosite (Str), near-phosphosite (Str), and away from phosphosite (Str). ** signifies significant differences in distributions (two-sample KS tests and t tests, p-value < 0.01). (D) Example case of phosphomannomutase, presenting superimposed and aligned structures of the phosphorylated (PDB ID 2FKF, colored dark cyan) and unphosphorylated (PDB ID 2FKM, colored yellow) forms. Dashed circles highlight notable structural changes at the phosphosite and away from it.

contribute to a more comprehensive understanding of the consequential change in the conformational landscape of proteins, associated with the phosphorylation events.

Phosphorylation-induced conformational changes refer to alterations in the three-dimensional structure of proteins upon the addition of a phosphate moiety to the protein. These changes can impact the overall folding of the protein or specific regions, leading to modifications of its functional properties. For instance, phosphorylation may induce conformational shifts that expose or conceal binding sites, influencing the interaction of protein with other molecules such as substrates, cofactors, or other proteins in a signaling cascade.[10] Phosphorylation not only affects static conformation, but it can also introduce dynamic changes in protein behavior.[11] Proteins are not rigid structures; rather, they exhibit inherent flexibility and dynamic motion. Phosphorylation can influence these dynamic properties by altering the vibrational modes, flexibility, and motion within the protein structure. This dynamic modulation is essential for fine-tuning of cellular processes, allowing for rapid and precise responses to various stimuli. Understanding how phosphorylation impacts protein dynamics provides insight into the temporal aspects of cellular signaling and regulatory mechanisms. Phosphorylation-induced changes extend beyond the core of the protein structure to its surface properties, specifically alterations in the accessible surface area (ASA). The addition of a phosphate group can expose or shield specific regions on the protein surface, influencing its interactions with solvent molecules, other proteins, and cellular membranes. These ASA changes are crucial for mediating protein−protein interactions, subcellular localization, and interactions with ligands.[12] By modulation of the ASA, phosphorylation contributes to the spatiotemporal regulation of cellular events and ensures the precise orchestration of signaling cascades. The study also underscores the centrality of eukaryotic phosphorylation on serine, threonine, and tyrosine residues as a fundamental mechanism for regulating diverse cellular processes. Each type of phosphorylation, coupled with its distinct location on the amino acid residues, has specific implications for protein structure, function, and cellular signaling. This nuanced understanding is paramount for unraveling the complexities of cellular regulation and holds the key to developing targeted therapeutic strategies.

Our current study takes a systematic approach to explore the prevalence, extent, location, and functional relevance of conformational alterations induced by phosphorylation at a single residue position. Analyzing a non-redundant data set of 24 proteins in both phosphorylated and unphosphorylated states, our study showcases distinct conformational changes occurring away from the phosphorylation site. Furthermore, we shed light on dynamic shifts in protein residues, emphasizing the long-range impact of phosphorylation on protein dynamics. The investigation also reveals how phosphorylation affects the

https://doi.org/10.1021/acsomega.4c00523
ACS Omega 2024, 9, 24520−24537

residue motion correlation and perturbs low-frequency global modes in the unphosphorylated form. Notably, observable differences in the total accessible surface postphosphorylation are accentuated in the vicinity of the phosphorylation site, underlining the localized impact on surface properties. To provide a more granular understanding, the study delves into two case studies spanning phosphorylation of serine, threonine, and tyrosine. The first case demonstrates how phosphorylation at different protein sites induces variable structural and dynamic changes, potentially impacting function. In the second case, we elucidate how phosphorylation within a kinase's activation loop brings about functional changes by influencing its structure and dynamics.

RESULTS

Protein Structures Undergo Distinct Conformational Changes upon Phosphorylation, with More Pronounced Alterations Occurring away from the Site of Phosphorylation. The SSP (single-site phosphorylation) data set, comprising 24 pairs of phosphorylated and unphosphorylated states of proteins, phosphorylated at a single serine, threonine, or tyrosine residue was specifically curated from the RCSB Protein Data Bank (Table S1). Criteria for curation and workflow are outlined in Supplementary Figure 1A (refer to Methods). In the SSP data set, the phosphate moiety or modified protein residue showed a predominant presence in the loop region, accounting for 50% (12 out of 24 occurrences), followed by the helix region at 42% (10 out of 24), and with a smaller representation in the β-sheet region at 8% (2 out of 24) (Supplementary Figure 1B). Upon normalization, as detailed in the Methods section, and taking into account the inherent occurrence propensities of helices, β-strands, and loops, the probability of a phosphorylated residue occurring in helices was calculated to be 44% (propensity = 1.192); in β-strands, it was 18% (propensity = 0.5), and in loops, it was 38% (propensity = 1.033) (Supplementary Figure 1C). This normalization allows us to present a more nuanced and accurate depiction of the distribution of phosphorylated sites in our data set across different secondary structures. Post data set curation, the Cα-root-mean-square deviation (RMSD) between phosphorylated and unphosphorylated states was computed for each protein pair in the SSP data set. Notably, 18 out of 24 proteins (~75% of the data set) exhibited significant structural differences (Figure 1A). Significance was determined by considering RMSD values exceeding the standard deviation from the mean of RMSDs observed in the control data set. All protein pairs had a TM-score value, higher than 0.5, indicating overall fold similarity (Supplementary Figure 2A). We compared the Cα-RMSD distribution of the SSP data set with that of the control data set in order to take into account the impact of crystal packing on the protein structure. The two distributions were found to be significantly different (two-sample Kilmogorov−Smirnov [KS] tests and t tests, $p < 10^{-2}$), indicating that phosphorylation modification of the protein, rather than crystallization artifacts, is the primary cause of the observed changes in global protein conformation (Figure 1B,C).

We categorized the residues into phosphosite (Seq), non-phosphosite (Seq), phosphosite (Str), near-phosphosite (Str), and away from phosphosite (Str) residues to identify specific regions undergoing conformational alterations linked to the phosphorylation event (refer to Methods). RMSD was computed independently for these residue segments. This allowed us to comprehensively delineate the local structural differences between the phosphorylated and unphosphorylated states. The distribution of RMSD for both phosphosite (Seq) and non-phosphosite (Seq) residues exhibited a statistically significant difference (two-sample Kilmogorov-Smirnov [KS] tests and t tests, $p < 10^{-2}$) compared to the control data set (Figure 1B). This distinction was also observed in the case of phosphosite (Str), near-phosphosite (Str), and away from phosphosite (Str) with respect to the control data set (Figure 1C). Upon careful analysis of the plots (Figure 1B,C and Supplementary Figure 2B,C, which includes outliers), it was observed that there are considerable structural differences between the phosphorylated and unphosphorylated forms at the phosphosite. Additionally, significant RMSD variations were found in the regions surrounding the phosphorylation site, both proximal and distal, with the disparities being more prominent in the latter case. A specific instance of the protein phosphomannomutase, representing superimposed and aligned structures of both the phosphorylated (PDB ID 2FKF) and unphosphorylated (PDB ID 2FKM) forms, highlights notable structural changes at the phosphosite and in regions distal to it (Figure 1D) with the Cα-RMSD being 0.77 Å. For sequence-based classified regions, the RMSD is 0.67 Å at the phosphosite and 0.78 Å at the non-phosphosite, while for structure-based classification, the RMSD is 0.58 Å at the phosphosite, 0.68 Å for the near-phosphosite, and 0.8 Å for residues away from phosphosite.

Phosphorylation Induces Dynamic Shifts in Protein Residues, with Notable Effects Extending Further from the Phosphorylation Site, Highlighting Its Long-Range Impact on Protein Dynamics. Protein flexibility is a result of energetically feasible intrinsic functional motions encoded within their tertiary structures. These intrinsic motions, crucial for understanding the dynamic behavior of biomolecules, are often investigated using normal mode analysis (NMA).[9,13] By studying the vibrational motion of a harmonic oscillating system in the immediate vicinity of its equilibrium, NMA provides insights into the inherent structural dynamics of proteins. The structural flexibility of proteins, evident in their normal modes, plays a pivotal role in facilitating functionally important conformational variations.[14,15] Coarse-grained normal mode analysis (NMA) has emerged as a potent tool in recent studies for probing protein dynamics across various fronts, offering a nuanced understanding of structural dynamics and functional mechanisms while being computationally efficient. Recent investigations have employed NMA to dissect the regulatory intricacies of muscle myosin ATPase,[16,17] unveil the dynamic interplay during RNA polymerase cycles,[18] elucidate the fundamental mechanisms of ribosomal machinery,[19,20] explore the nuanced behaviors of kinases and pseudokinases,[13] and model the structural dynamics of the SARS-CoV-2 Spike protein and many more research domains, revealing insights into intricate biological processes while acknowledging the inherent complexity of protein systems.[21]

In order to explore the nuanced differences in residue dynamics between phosphorylated and unphosphorylated forms of the proteins, we conducted detailed analyses on the normalized square fluctuations obtained through anisotropic network model-based normal mode analysis (ANM-NMA) on 34 (17 × 2) protein structures within the SSP data set, after filtering out and excluding cases with missing residues in either the phosphorylated or unphosphorylated forms of the proteins (refer to Methods). The difference in distribution of the absolute difference in normalized square fluctuations between

https://doi.org/10.1021/acsomega.4c00523
ACS Omega 2024, 9, 24520−24537

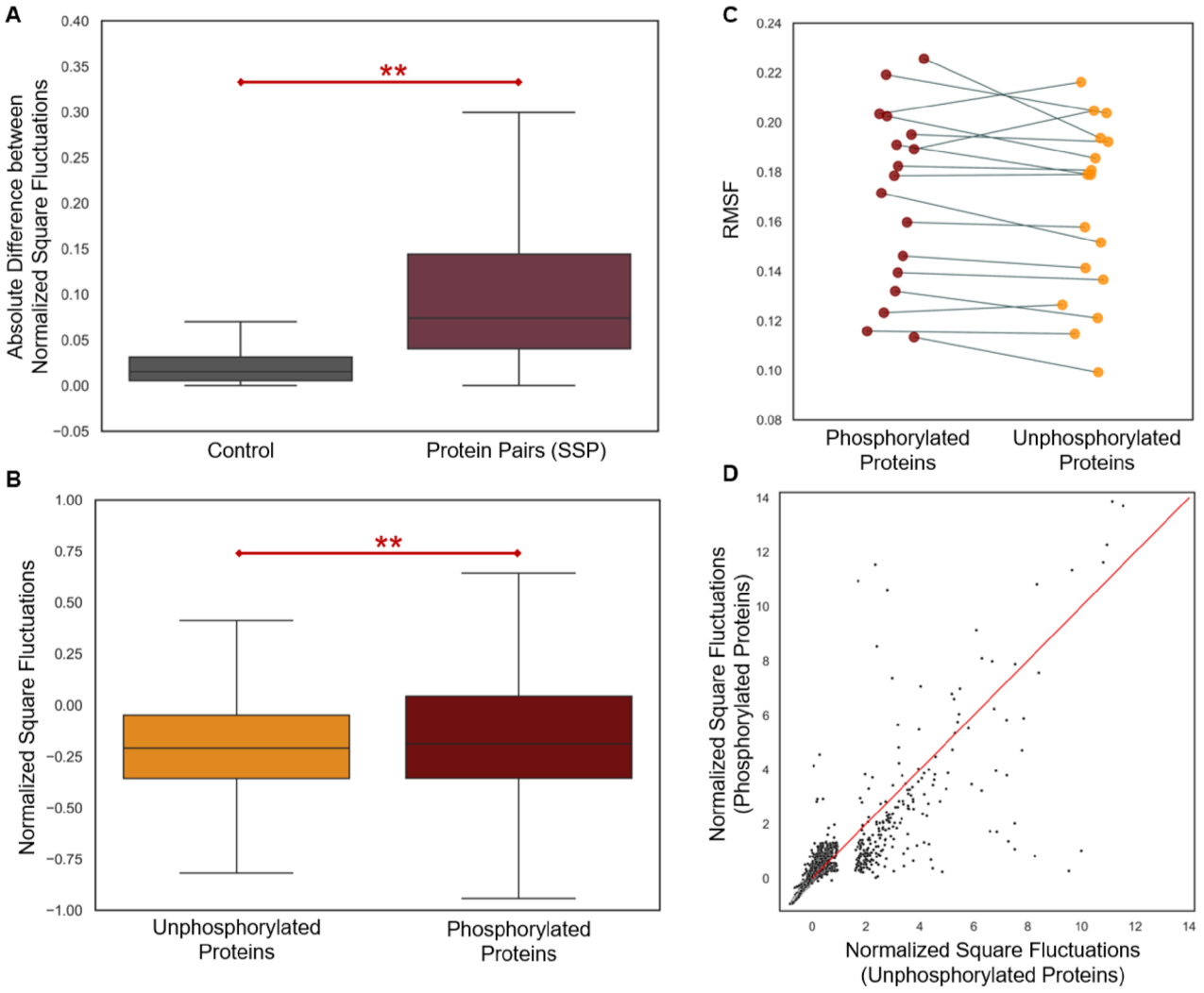

Figure 2. Dynamic shifts. (A) Box plots illustrating the distribution of the absolute difference in normalized square fluctuation of proteins between the control data set and the phosphorylated/unphosphorylated forms in the SSP data set. (B) Box plot displaying the distribution of normalized square fluctuations for all residues in phosphorylated and unphosphorylated proteins. ** indicates significant differences (two-sample KS tests, $p < 0.01$). (C) Paired strip plot of RMSF values for corresponding phosphorylated and unphosphorylated proteins in the SSP data set. (D) Scatter plot presenting the fluctuations for all residues in phosphorylated and unphosphorylated forms, aiding in the identification of residues exhibiting increased or decreased fluctuations (correlation coefficient: 0.75).

the phosphorylated and unphosphorylated forms was found to be statistically significant (two-sample KS tests, p-value $< 10^{-2}$), compared to the control group (Figure 2A and Supplementary Figure 4A, which includes outliers). Additionally, the distribution of normalized square fluctuation across all residues of phosphorylated proteins was significantly different (two-sample KS tests, p-value $< 10^{-2}$) from that of unphosphorylated proteins (Figure 2B and Supplementary Figure 4B, which includes outliers). This suggests that phosphorylated proteins exhibit altered flexibility in numerous residues post-phosphorylation, as indicated by a greater variance in fluctuation distribution. Upon further scrutiny, it was observed that the majority of the phosphorylated proteins exhibited a modestly higher root-mean-square fluctuation (RMSF) compared to their unphosphorylated counterparts (Figure 2C). The observed increase in RMSF could reflect a greater adaptability of phosphorylated proteins to undergo conformational changes necessary for their specific functions. Moreover, the observed differences in RMSF might be indicative of a dynamic equilibrium between distinct conformational states in phosphorylated and unphosphorylated proteins. Phosphorylation events could introduce multiple conformations, reflecting a dynamic interplay between different structural states. This conformational diversity may be functionally relevant, allowing phosphorylated proteins to respond more effectively to various cellular cues and environmental changes. Furthermore, it could also be linked to the modulation of protein−protein interactions. Phosphorylation serves as a molecular switch, regulating the assembly and disassembly of protein complexes. The increased RMSF in phosphorylated proteins is associated with a greater capacity for dynamic interactions, facilitating transient binding and release of interacting partners. This adaptability is crucial for precise temporal and spatial regulation of cellular processes. While our observation highlights a consistent trend in higher RMSF for phosphorylated proteins, it is essential to note that the relationship between phosphorylation and RMSF is complex and context-dependent. The specific site of phosphorylation, the type of amino acid modified, and the local structural environment can all contribute to the observed variations. Even at an individual residue level, we observed a general

https://doi.org/10.1021/acsomega.4c00523
ACS Omega 2024, 9, 24520−24537

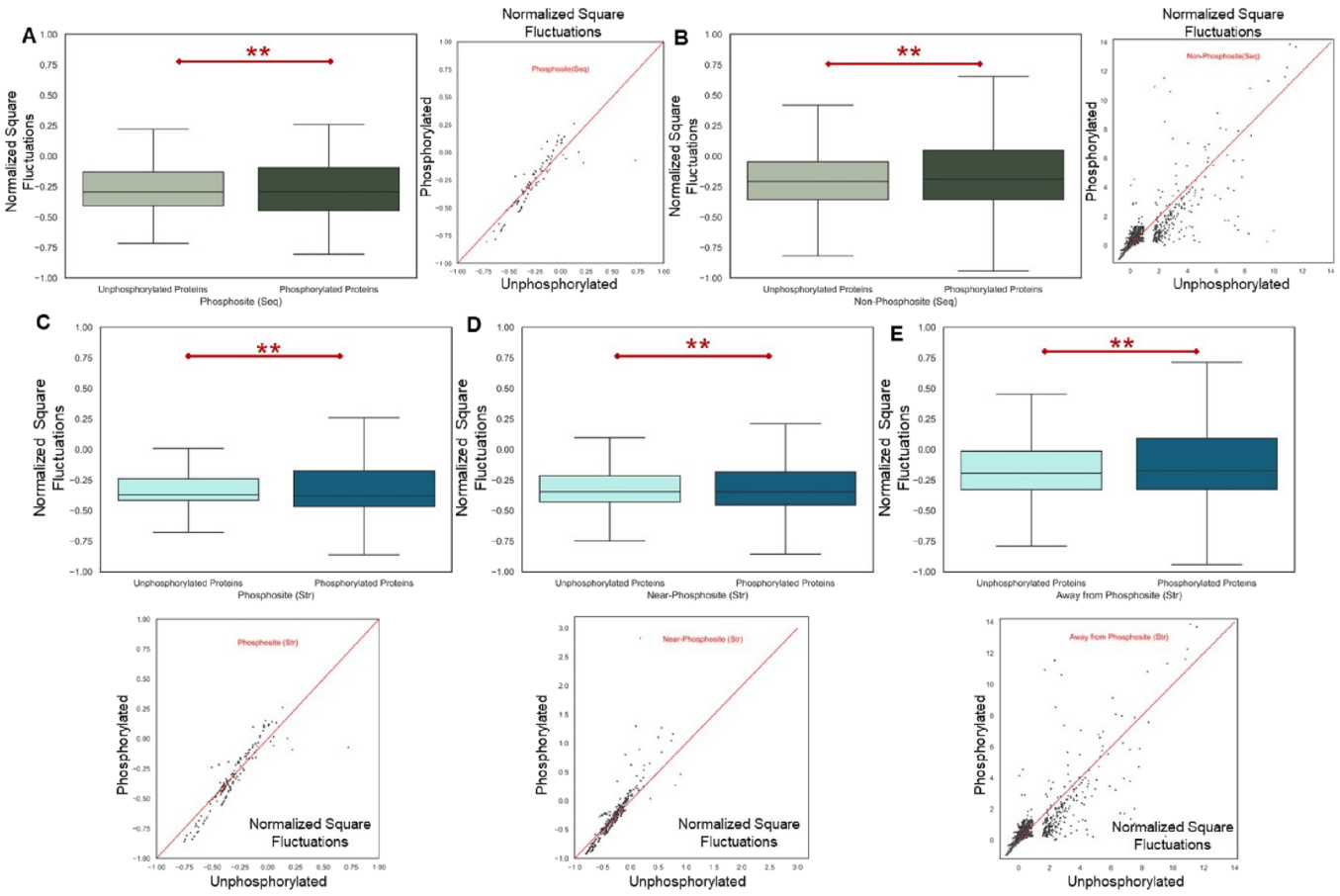

Figure 3. Localized regions showing changes in flexibility/dynamics post-phosphorylation. (A) Box plot (left) and scatter plot (right) (correlation coefficient: 0.9) showing normalized square fluctuations for phosphosite (Seq) residues in phosphorylated and unphosphorylated proteins. (B) Box plot (left) and scatter plot (right) (correlation coefficient: 0.75) illustrating normalized square fluctuations for non-phosphosite (Seq) residues in phosphorylated and unphosphorylated proteins. (C) Box plot (top) and scatter plot (bottom) (correlation coefficient: 0.9) presenting normalized square fluctuations for phosphosite (Str) residues in phosphorylated and unphosphorylated proteins. (D) Box plot (top) and scatter plot (bottom) (correlation coefficient: 0.83) displaying normalized square fluctuations for near-phosphosite (Str) residues in phosphorylated and unphosphorylated proteins. (E) Box plot (top) and scatter plot (bottom) (correlation coefficient: 0.74) depicting normalized square fluctuations for away from phosphosite (Str) residues in phosphorylated and unphosphorylated proteins. ** indicates significant differences (two-sample KS tests, $p < 0.01$).

increase in flexibility following phosphorylation (Figure 2D). To quantify the percentage of residues undergoing significant changes, the difference in residue fluctuations between phosphorylated and unphosphorylated forms was calculated. Significance was attributed only if the difference exceeded the standard deviation from the mean of the fluctuation difference in the control data set. The findings indicated that 3.4% of residues exhibited significantly higher fluctuation in the unphosphorylated form, while 1.4% of residues showed significantly higher fluctuation in the phosphorylated form. Certain specific regions, particularly in loop structures and occasionally in helices (e.g., residue 122 in lactoperoxidase, PDB ID 4QJQ) and β-strands (e.g., residues 300−301 in pepsin, PDB ID 4PEP, and residue 88 in MYT1 kinase, PDB ID 5VCV), exhibited pronounced deviation in normalized square fluctuations post-phosphorylation. These deviations might suggest a potential role for these residues in enabling dynamic shifts essential for protein's functions. For instance, in the case of the protein glycogen synthase kinase-3 beta, residues 48 and 50, which are part of the glycine-rich loop, responsible for binding and positioning ATP for phosphotransfer, displayed high fluctuation deviations. Similarly, in Pim1, residue 82 shows notable fluctuation deviation with documented mutations (N82K) resulting in decreased kinase activity, emphasizing the functional significance of this region.[16] However, many of these highly fluctuating residues lack comprehensive functional annotations in the existing literature. Moreover, some outliers exhibit high B-factors, rendering them akin to missing residues. Nonetheless, given the relatively small proportion of these outliers, their impact on our analysis is negligible. Specifically, when RMSF is computed, its presence does not exert a substantial influence on the overall results. This is because RMSF entails calculating the square root of the mean of squared fluctuations, and the averaging effect mitigates the impact of outliers on the overall analysis. Consequently, the presence of outliers does not contribute significantly to the meaningful details of our analysis.

To ensure the robustness of these differences, irrespective of the 15 Å distance cutoff used for normal mode analysis (NMA) calculations, additional analyses were conducted. Normalized fluctuations of phosphorylated and unphosphorylated proteins in the SSP data set, as well as all proteins in the control data set, were calculated at 12 and 10 Å cutoffs. The absolute difference in fluctuations between the control and SSP data set (Supplementary Figure 3A), as well as the fluctuations in phosphorylated and unphosphorylated forms (Supplementary Figure 3B), remained consistently significant at 12 and 10 Å cutoffs,

https://doi.org/10.1021/acsomega.4c00523
ACS Omega 2024, 9, 24520−24537

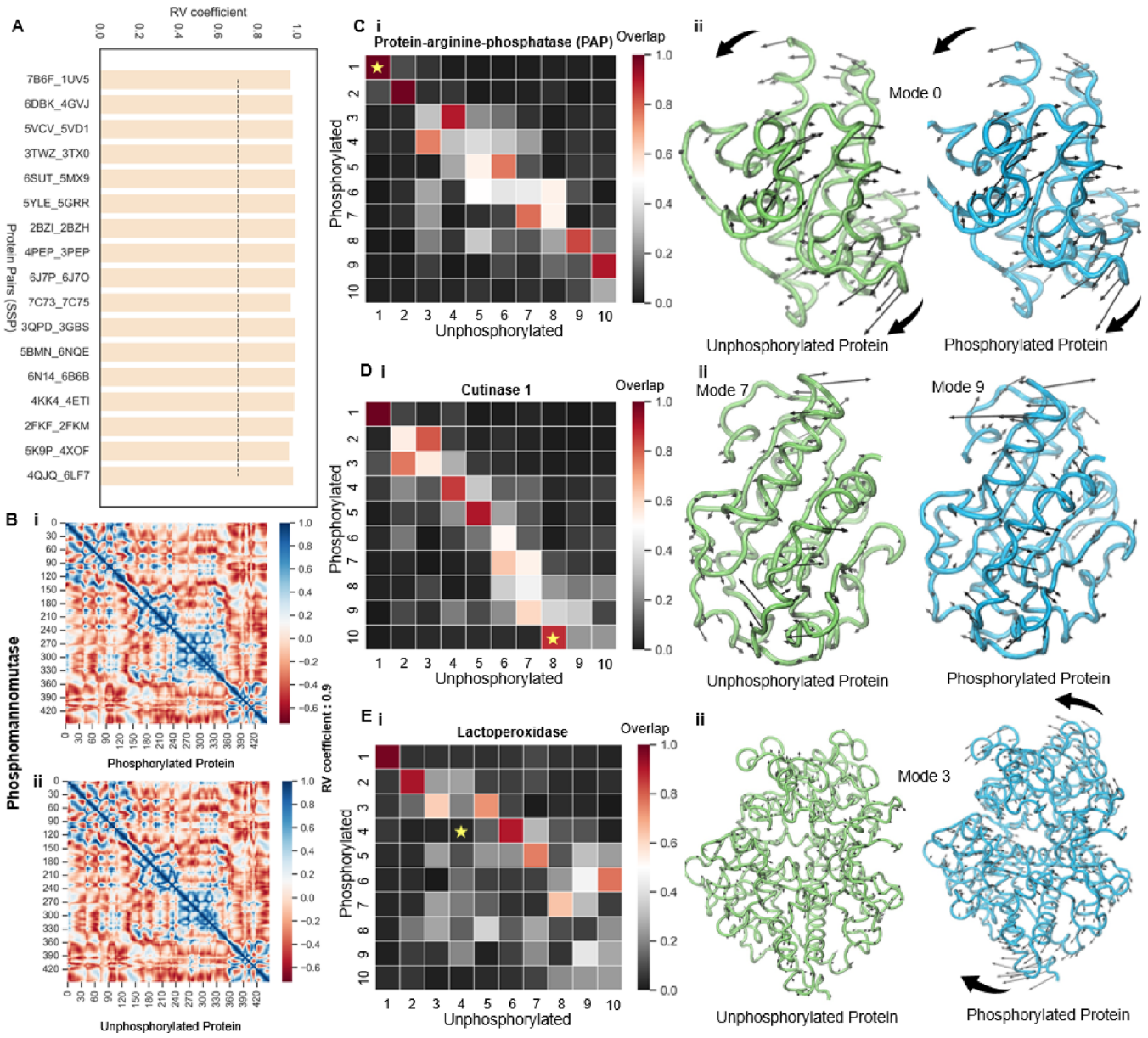

Figure 4. Cross-correlation analysis and overlap analysis for proteins in the SSP data set. (A) Bar plot representing the similarity between cross-correlation matrices of phosphorylated and unphosphorylated proteins. The black horizontal line denotes the similarity cutoff. (B) Example case from the SSP data set featuring phosphomannomutase (PDB ID 2FKF, phosphorylated; PDB ID 2FKM, unphosphorylated) where phosphorylation does not alter residue communication. The cross-correlation matrices show a high similarity (R_v coefficient = 0.9). (C) (i) Overlap of the first 10 nonzero normal modes of phosphorylated and unphosphorylated forms of protein-arginine-phosphatase (PAP). (ii) Backbone fluctuations indicated by eigenvectors of the unphosphorylated protein (left) and phosphorylated protein (right) for mode 1. (D) (i) Overlap of the first 10 nonzero normal modes of phosphorylated and unphosphorylated forms of cutinase 1. (ii) Backbone fluctuations indicated by eigenvectors of the unphosphorylated protein (left) for mode 8 and the phosphorylated protein (right) for mode 10. (E) (i) Overlap of the first 10 nonzero normal modes of phosphorylated and unphosphorylated forms of lactoperoxidase. (ii) Backbone fluctuations indicated by eigenvectors of the unphosphorylated protein (left) and phosphorylated protein (right) for mode 4. * denotes the investigated mode, and thick arrows indicate major collective motions.

indicating that these observed variations were insensitive to the chosen distance cutoff. These observations highlight a discernible post-phosphorylation augmentation in the dynamic motion of residues, signifying an enhanced level of structural flexibility.

The fluctuation profiles of phosphorylated and unphosphorylated proteins were subjected to separate analyses across distinct residue categories: Phosphosite (Seq), non-phosphosite (Seq), phosphosite (Str), near-phosphosite (Str), and away from phosphosite (Str) (Figure 3). The objective was to pinpoint specific areas undergoing dynamic shifts associated with the phosphorylation modification event. In all regions, phosphosite (Seq) (Figure 3A), non-phosphosite (Seq) (Figure 3B), phosphosite (Str) (Figure 3C), near-phosphosite (Str) (Figure 3D), and away from phosphosite (Str) (Figure 3E), the distributions of normalized square fluctuations of phosphorylated proteins were found to be significantly different (two-sample KS tests, p-value $< 10^{-2}$) compared to their unphosphorylated counterparts (Supplementary Figure 4C,D, which includes outliers). Notably, phosphorylated proteins exhibited a marginally heightened level of flexibility[11] across all the aforementioned regions, with a particularly noteworthy

https://doi.org/10.1021/acsomega.4c00523
ACS Omega 2024, 9, 24520−24537

observation near the phosphorylation sites. In this specific region, near-phosphosite (Str), 1.1% of residues exhibited a significantly higher fluctuation in the phosphorylated proteins, compared to only 0.2% in their unphosphorylated counterparts.

Protein Phosphorylation Does Not Significantly Change the Residue Motion Correlation, but It Perturbs the Low-Frequency Global Modes in the Unphosphorylated Form. Exploring the repercussions of protein phosphorylation on the residue motion correlation is crucial for gaining insights into the complexities of residue communication within a protein. Correlated fluctuations among residues serve as conduits for vital information transmission, and identifying residues with coupled motion is instrumental in deciphering functional pathways.[17] Residue−residue cross-correlation matrices were computed for both phosphorylated and unphosphorylated forms of proteins in the SSP data set, for cases where ANM-NMA analyses were performed. The R_v coefficient, calculated between the cross-correlation matrices of phosphorylated and unphosphorylated protein pairs, served as a quantitative measure to estimate similarity/dissimilarity between correlated motions in both the forms. The coupling between residue fluctuations appeared to be largely unaffected post-phosphorylation, as indicated by high R_v coefficients ($\geq$0.7) (Figure 4A). Figure 4B illustrates an example from the data set featuring the protein phosphomannomutase, where phosphorylation has no significant impact on the residue−residue correlation, as evidenced by a high R_v coefficient of 0.9. The conserved correlation patterns observed in our study suggest the potential resilience of certain communication pathways and cooperative interactions among residues, even in the presence of phosphorylation events. While our findings hint at a stable network of correlated fluctuations, it is important to acknowledge the limitations inherent in our data set, which primarily comprises stable and well-behaved protein structures. These structures, while informative, may not fully capture the dynamic nature of protein behavior in vivo and might not represent the entire picture. Hence, a more comprehensive data analysis with a larger data set would be necessary in the future to provide a clearer understanding, particularly with the potential increase in available crystal structures in the PDB.

Low-frequency global modes derived from the normal mode analysis (NMA) have emerged as crucial indicators of biologically relevant dynamics in proteins. They provide insightful information about how these biomolecules function. A previous study has underscored the significance of these modes in governing the enzymatic activity, substrate binding, and conformational changes. For instance, Marcos et al. demonstrated that enzymes within the amino acid kinase family acquire new modes of motion upon oligomerization.[18] This structural rearrangement plays a pivotal role in regulating substrate binding, highlighting the significance of low-frequency modes in the enzymatic function. In a different study, Oliwa and Shen attempted to model conformational changes that occur upon binding by re-evaluating and reordering normal modes.[19] This approach aimed to capture the dynamic rearrangements associated with the recognition and binding. Furthermore, investigations have revealed that the low-frequency global modes of unbound proteins are perturbed upon interaction with their binding partners.[9] This phenomenon sheds light on the influence of binding events on the conformational dynamics of proteins.

Building upon these findings, it becomes intriguing to explore the impact of post-translational modifications, such as phosphorylation, on low-frequency global modes. Deciphering whether phosphorylation alters the low-frequency modes of proteins and how these modifications relate to functional dynamics will be crucial to understanding the complex mechanisms that underlie cellular functions. To address this question, we conducted a comprehensive analysis to determine whether phosphorylation introduces new low-frequency motions or preserves the inherent dynamics of proteins. Our approach involved analyzing the similarities and differences between the modes of motion accessible to a protein in its phosphorylated and unphosphorylated forms. This was done by quantifying the overlap between the top 10 low-frequency global motions obtained from NMA. The overlap value serves as a robust indicator of the similarity between modes in terms of their frequency, shape, and size. A smaller overlap value signifies a larger difference in the two modes of motion. Significantly, low-frequency global modes showed little overlap in about 71% of the cases in our study, suggesting a substantial shift in mode preference and order upon phosphorylation. A shift in mode preference implies that a mode "m", present as a low-frequency mode in one form, manifests as the same or a similar mode (defined by a high overlap value) in the other form but with a modified frequency. This finding suggests that while some modes of motion are preserved between the phosphorylated and unphosphorylated forms, their frequency, size, and shape undergo substantial changes, as evidenced by the reordering of normal modes. The introduction of a phosphate moiety not only alters the low-frequency modes of proteins but also imparts distinct character to their functional dynamics. We examined several case examples to provide concrete evidence of the impact of phosphorylation on low-frequency global modes of proteins. One such case involved protein-arginine-phosphatase (PAP), where we observed that the mode order was retained for the first low-frequency mode, as indicated by a high overlap value (Figure 4C,i). We observed that the major collective motions of the phosphorylated and unphosphorylated forms were alike, based on the eigenvectors representing the corresponding backbone fluctuation for mode 1 (Figure 4C,ii). Another case study focused on cutinase 1, where we observed a clear instance of mode reordering. Specifically, the eighth mode of the unphosphorylated form manifested as the tenth mode of the phosphorylated protein, as indicated by high overlap values (Figure 4D,i). To provide further insight, we examined the corresponding eigenvectors for backbone fluctuation in mode 8 of the unphosphorylated protein and mode 10 of the phosphorylated protein, showcasing a notable degree of comparability (Figure 4D,ii). Additionally, we investigated the case of lactoperoxidase, where we found that global mode 4 of the unphosphorylated form was not preserved in the phosphorylated form (Figure 4E,i). This evidence was supported by the eigenvectors for backbone fluctuation in mode 4 of the unphosphorylated and phosphorylated forms. Notably, the low-frequency motions observed in the unphosphorylated form are lost, and new collective motions are introduced post-phosphorylation, as evident in the phosphorylated protein (Figure 4E,ii). The aforementioned case studies collectively provide insight into the diverse effects of phosphorylation on low-frequency global modes, ranging from preserved mode characteristics in PAP to mode reordering in cutinase 1 and the introduction of new collective motions in lactoperoxidase.

These observations unveil a fascinating duality in the impact of phosphorylation on the protein dynamics. First, the stability

https://doi.org/10.1021/acsomega.4c00523
ACS Omega 2024, 9, 24520−24537

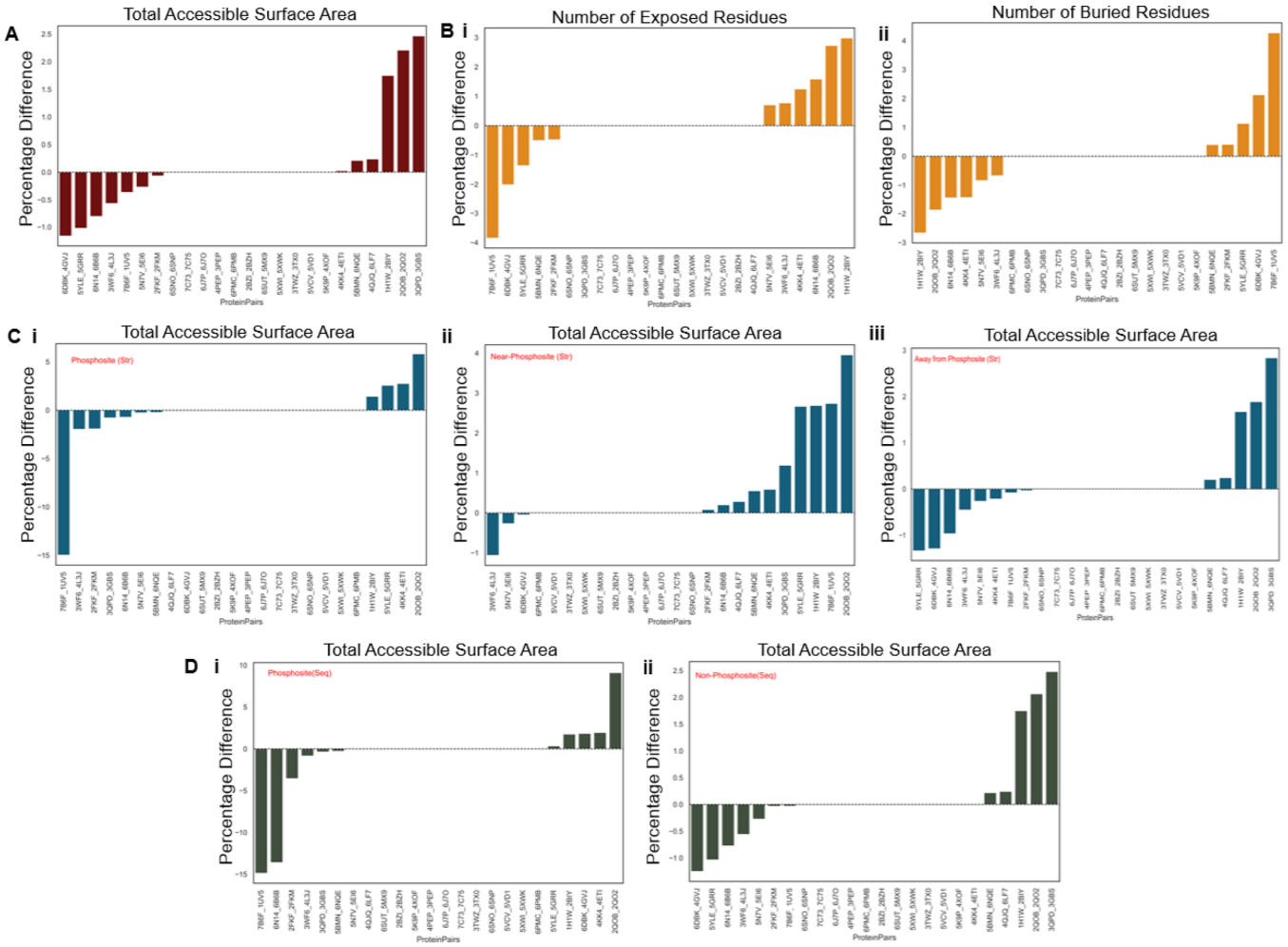

Figure 5. ASA analyses. (A) Percentage change in the total accessible surface area for all proteins. (B) Percentage difference (i) in the number of exposed residues post-phosphorylation and (ii) in the number of buried residues post-phosphorylation. (C) Percentage change in the total accessible surface area considering all (i) phosphosite (Str) residues, (ii) near-phosphosite (Str) residues, and (iii) away from phosphosite (Str) residues. (D) Percentage change in the total accessible surface area: (i) the phosphosite (Seq) region and (ii) the non-phosphosite (Seq) region. Protein pairs above the black line indicate an increase in the surface area post-phosphorylation, while protein pairs below the line show a reduction.

in the residue motion correlation despite phosphorylation implies that the local interactions and coordinated movements between residues remain relatively unchanged. This suggests a certain robustness in the residue-level dynamics, indicating that phosphorylation may not disrupt the inherent correlations between residues. On the other hand, the perturbation of low-frequency global modes in the unphosphorylated form following phosphorylation reveals a nuanced and intricate alteration in the collective motions of the protein. While the residue-level interactions may remain stable, the larger-scale, global modes of motion are distinctly influenced by phosphorylation. This implies that the post-translational modification introduces changes in the collective, low-frequency dynamics of the protein, potentially impacting its overall structural and functional behavior. In essence, this duality in the observed effects of phosphorylation highlights the complexity of its influence on protein dynamics.

Observable Differences in the Total Accessible Surface Post-Phosphorylation Are Particularly Accentuated in the Vicinity of the Phosphorylation Site. The total accessible surface area (ASA) of a protein refers to the combined surface area of all of the atoms in the protein that are accessible to the surrounding solvent molecules. It is a measure of the exposed surface area and can help in understanding the interactions of the protein with other molecules such as ligands, substrates, or other proteins. Changes in the ASA can have significant implications for biological activity and its interactions within cellular environments. We sought to better understand the impact of phosphorylation on the total accessible surface area (ASA) of proteins, focusing on identifying the specific regions that undergo the most significant changes. We used NetPhos 3.1, a machine learning model trained on a diverse set of experimentally verified phosphorylation events to calculate the ASA values for both phosphorylated and unphosphorylated protein states within the SSP data set (refer to Methods). The exposed and buried residues were distinguished by applying a threshold of 25% relative accessible surface area (RASA). We separately computed the total ASA across distinct residue categories for all protein pairs in the SSP data set, phosphosite (Seq), non-phosphosite (Seq), phosphosite (Str), near-phosphosite (Str), and away from phosphosite (Str). By comparing the ASA values before and after phosphorylation, we were able to determine the percentage change in the total ASA for the entire protein, as well as for specific regions of interest.

https://doi.org/10.1021/acsomega.4c00523
ACS Omega 2024, 9, 24520−24537

Our findings revealed that 54% of the proteins exhibited a change in the total accessible surface area following phosphorylation. Among these proteins, 25% displayed an increase in the total ASA, while 29% showed a decrease (Figure 5A). Notably, 21% of proteins exhibited an augmented number of buried residues coupled with a decrease in the number of exposed residues, whereas 25% displayed an increase in the number of exposed residues and a corresponding decrease in the number of buried residues (Figure 5B). Zooming in on specific regions, we observed alterations at the phosphosite (Str) region, where approximately 46% of proteins demonstrated a change in the total ASA. Within this category, 17% experienced an increase, while 29% exhibited a decrease in the total ASA post-phosphorylation (Figure 5C,i). In the near-phosphosite (Str) region, we noted a substantial 54% showing a percentage difference in the total ASA, with a noteworthy 42% of proteins displaying an increase and only 12% showing a reduction (Figure 5C,ii). This region exhibited a pronounced skew, signifying a substantial disparity between the phosphorylated and unphosphorylated states. In the away from phosphosite (Str) region, we observed that 54% of the proteins exhibited a percentage difference in the total ASA, with 21% showing an increase and 33% showing a decrease (Figure 5C,iii). In the phosphosite (Seq) region, approximately 46% of proteins displayed a change, with 21% experiencing an increase and 25% demonstrating a decrease (Figure 5D,i). Finally, in the non-phosphosite (Seq) region, 50% of proteins showcased a difference, with 21% indicating an increase and 29% showing a decrease (Figure 5D,ii).

By altering the surface accessibility of residues, phosphorylation can regulate protein−protein interactions, signaling pathways, and cellular processes. Based on our analysis, phosphorylation has a notable impact on the accessible surface area (ASA) of proteins. The observed variations in accessible surface area (ASA) post-phosphorylation provide valuable insights into the dynamic nature of protein modifications and their impact on protein structure and function. The increase in the total ASA for a subset of proteins suggests that phosphorylation can lead to a more exposed and accessible surface. This phenomenon may be attributed to conformational changes triggered by phosphorylation, exposing previously buried residues to the solvent and potentially facilitating interactions with other molecules or proteins. Conversely, proteins that demonstrated a reduction in the total ASA post-phosphorylation imply a more compact or shielded structure. This could be indicative of phosphorylation-induced structural rearrangements that result in a tighter packing of residues or a shielding effect on certain regions of the protein, potentially protecting them from further modifications or interactions. The region-specific differences, particularly in the near-phosphosite (Str) category, highlight the intricate and context-dependent nature of phosphorylation effects. The substantial skew in this region, with a majority of proteins showing an increase in the total ASA, implies a pronounced impact of phosphorylation on creating more exposed surfaces in the proximity of phosphorylation sites, indicating its crucial role in the structural and functional consequences of phosphorylation.

Alterations in the ASA, following phosphorylation, may have potential ramifications on the stability of the protein molecule. In the context of stability, a decrease in the level of the ASA may suggest a potentially more compact conformation, contributing to improved structural stability. This potential enhancement can be attributed to a reduced level of exposure of hydrophobic regions to the solvent, minimizing potential destabilizing interactions. For instance, in the case of the protein probable phosphatidylethanolamine transferase Mcr-1, a reduction in the ASA post-phosphorylation corresponds to an energetically more stable phosphorylated form (PDB ID 5YLE, total energy = −14,166.184 kJ/mol, comprising bond = 709.529, angles = 1524.035, torsion = 1644.771, improper = 278.325, nonbonded = −9963.1, and electrostatic = −8359.74) compared to the unphosphorylated form (PDB ID 5GRR, total energy = −12,559.741 kJ/mol, comprising bond = 886.619, angles = 1838.175, torsion = 1643.839, improper = 309.454, nonbonded = −10,183.72, and electrostatic = −7054.1). Conversely, an increase in the ASA may potentially impact molecular interactions, influencing the stability of the phosphorylated form. Solvent-accessible regions may potentially become more susceptible to factors, such as solvent-mediated effects or interactions with other molecules. For instance, in the protein cutinase 1, where an increase in the ASA post-phosphorylation is observed, the unphosphorylated form (PDB ID 3GBS, total energy = −6757.094 kJ/mol, comprising bond = 209.419, angles = 851.655, torsion = 657.033, improper = 160.414, nonbonded = −4892.12, and electrostatic = −3743.5) is energetically more stable than the phosphorylated form (PDB ID 3QPD, total energy = −6256.449 kJ/mol, comprising bond = 632.74, angles = 980.399, torsion = 868.67, improper = 288.223, nonbonded = −5173.7, and electrostatic = −3852.68). However, it is crucial to note that the relationship between changes in the ASA and protein stability might not always be straightforward. Stability is a multifaceted attribute influenced by a myriad of factors, including but not limited to dynamic conformational changes, altered hydrogen bonding patterns, variations in intramolecular forces, and potential modifications in tertiary and quaternary structures. The observed changes in the ASA, while providing valuable insights, represent just one facet of the complex interplay influencing protein stability following phosphorylation events.

Phosphorylation at Different Protein Sites Induces Variable Structural and Dynamics Changes, Potentially Impacting Function: A Case Study on Polyubiquitin B. Polyubiquitin B is a protein that plays a crucial role in protein degradation through the ubiquitin-proteasome system. It can exist in different forms: covalently attached to another protein or free (unanchored). When covalently bound, it can be conjugated to target proteins as a monomer (monoubiquitin) or as a polymer linked via different lysine residues of the ubiquitin (polyubiquitin chains). The functional diversity of polyubiquitin chains is contingent upon the specific Lys residue to which ubiquitin is linked.[20] For example, Lys-6-linked chains may be involved in DNA repair, Lys-11-linked chains are associated with endoplasmic reticulum-associated degradation (ERAD) and cell cycle regulation, Lys-29-linked chains play a role in proteotoxic stress response and cell cycle,[21] Lys-33-linked chains are involved in kinase modification, Lys-48-linked chains are crucial for protein degradation via the proteasome, and Lys-63-linked chains participate in endocytosis, DNA-damage responses, and activation of the transcription factor NF-kappa-B. When existing as free entities, unanchored polyubiquitin molecules serve distinct roles, such as activating protein kinases and participating in signaling pathways. Phosphorylation of polyubiquitin B can occur on different residues, leading to diverse functional outcomes. The phosphorylation of specific residues influences the protein's activity and its interactions with other molecules. For instance, phosphorylation on certain

https://doi.org/10.1021/acsomega.4c00523
ACS Omega 2024, 9, 24520−24537

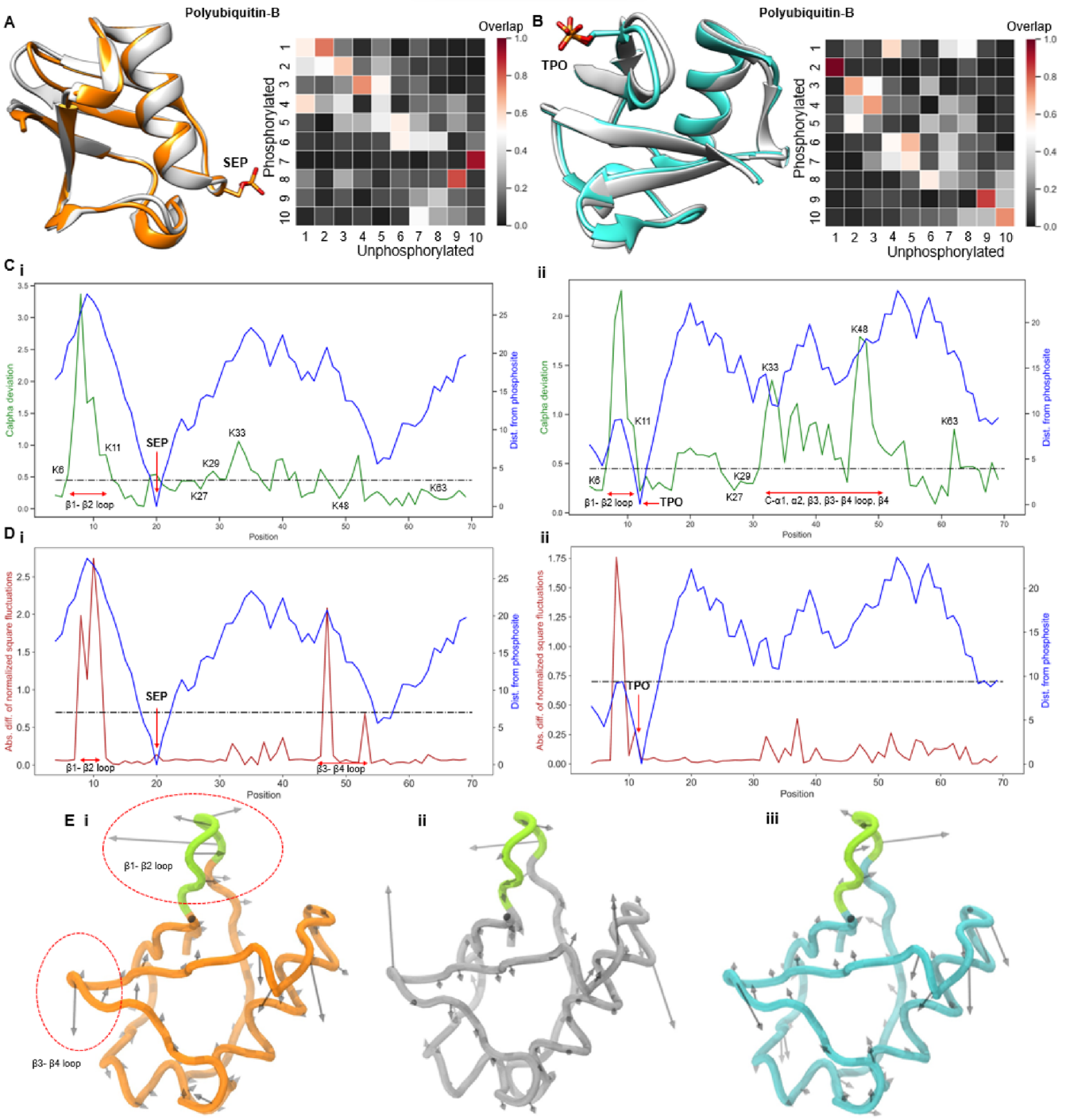

Figure 6. Understanding structure-dynamics alterations in polyubiquitin B. (A) Left: superimposed and aligned structures of Ser 20 phosphorylated (PDB ID 5K9P, colored orange) and unphosphorylated (PDB ID 4XOF, colored silver) forms. Right: overlap of the first 10 nonzero normal modes of both forms. (B) Left: superimposed and aligned structures of Thr 12 phosphorylated (PDB ID 5NVG, colored cyan) and unphosphorylated (PDB ID 4XOF, colored silver) forms. Right: overlap of the first 10 nonzero normal modes of both forms. (C) Cα-deviations between (i) Ser 20 phosphorylated and unphosphorylated forms and (ii) between Thr 12 phosphorylated and unphosphorylated forms for all aligned residues, denoted by a green line. (D) (i) Absolute difference between normalized square fluctuations of (i) Ser 20 phosphorylated and unphosphorylated forms and (ii) Thr 12 phosphorylated and unphosphorylated forms, for aligned residues, denoted by a maroon line. The blue line represents the distance of each residue from the phosphorylation site. The black line indicates the significance cutoff. Regions/residues of interest are marked in the plots. (E) Backbone fluctuations indicated by eigenvectors of mode 9 for the Ser 20 phosphorylated form (left), unphosphorylated form (middle), and Thr 12 phosphorylated form (right).

residues may modulate polyubiquitin B's ability to bind to RNA molecules. Disruption of RNA binding can significantly impact gene expression regulation and other cellular processes. Additionally, phosphorylation at Ser-65 has been shown to activate parkin (PRKN), triggering mitophagy.[22] It has also been observed that Ser-65 phosphorylation affects the discharging of E2 enzymes during the formation of polyubiquitin chains and can impact deubiquitination by enzymes like USP30.[23]

https://doi.org/10.1021/acsomega.4c00523
ACS Omega 2024, 9, 24520−24537

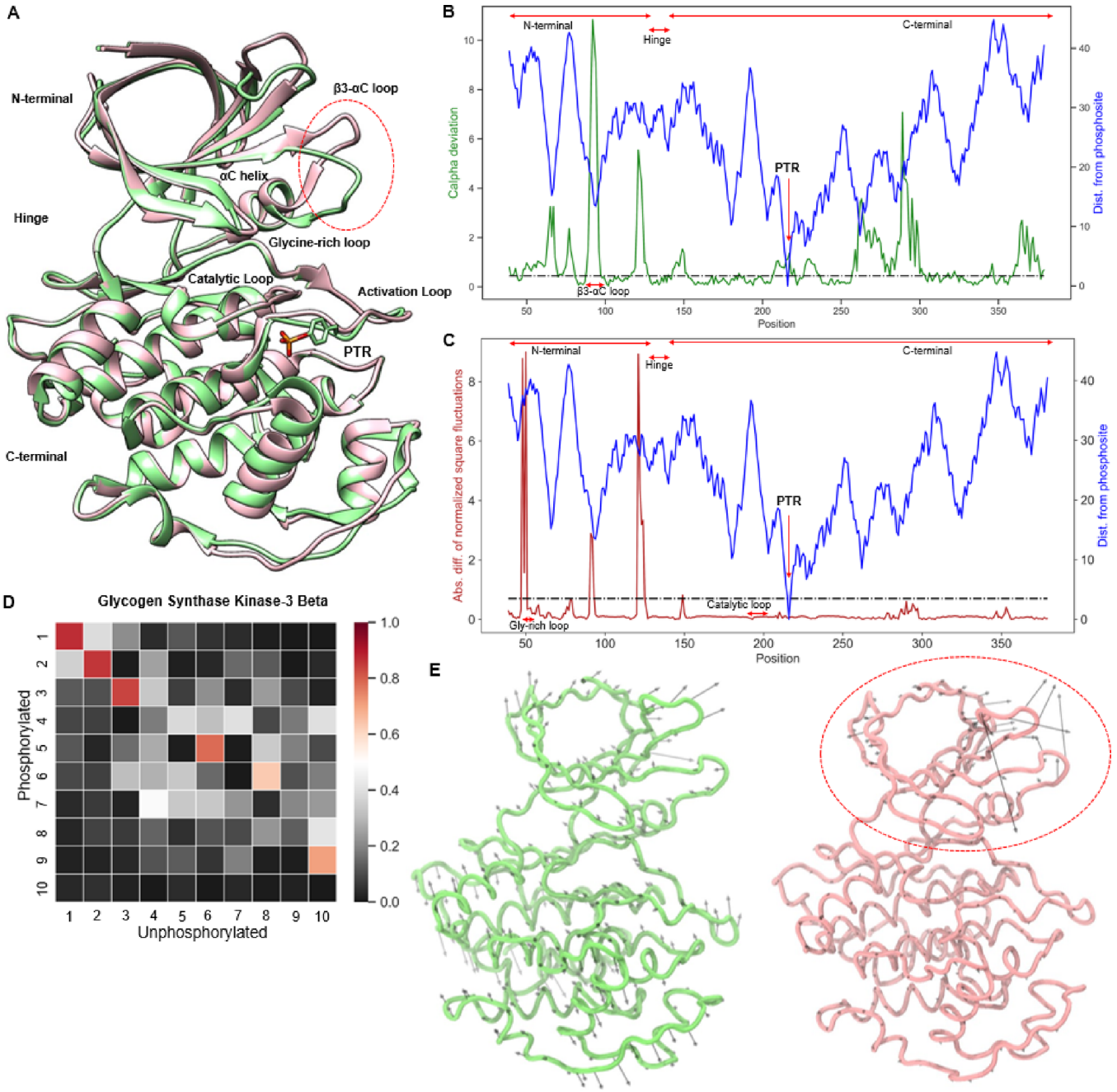

Figure 7. Phosphorylation induces changes in glycogen synthase kinase-3 beta. (A) Superimposed and aligned structures of Tyr 216 phosphorylated (PDB ID 7B6F, colored green) and unphosphorylated (PDB ID 1UV5, colored pink) forms of GSK-3β. Important regions of the kinase are marked, and the red circle indicates the region with significant structural disparities. (B) Cα-deviation between phosphorylated and unphosphorylated forms for all aligned residues, denoted by a green line. (C) Absolute difference between normalized square fluctuations of phosphorylated and unphosphorylated forms for aligned residues denoted by a maroon line. The blue line represents the distance of each residue from the phosphorylation site. The black line indicates the significance cutoff. Regions/residues of interest are marked in the plots. (D) Overlap of the first 10 nonzero normal modes of both phosphorylated and unphosphorylated forms. (E) Backbone fluctuations indicated by eigenvectors of mode 5 for the phosphorylated form (left) and the unphosphorylated form (right).

However, it is important to note that the current literature limits comprehensive insights into the distinct functional implications of phosphorylation on different residues, emphasizing the need for further research to elucidate the nuanced effects of residue-specific phosphorylation on polyubiquitin B.

In this study, we analyzed two phosphorylated forms of polyubiquitin B: one phosphorylated at the serine residue at position 20 (PDB ID 5K9P) (Figure 6A, left) and the other phosphorylated at the threonine residue at position 12 (PDB ID 5NVG) (Figure 6B, left), comparing them with the unphosphorylated polyubiquitin B structure (PDB ID 4XOF). To assess the structure-dynamics changes, we performed structural alignments of the phosphorylated forms with the unphosphorylated forms and computed the Cα-deviation and absolute difference of normalized square fluctuations for the aligned residues. We observed that phosphorylation perturbed the low-frequency global modes of the protein, evident from the low overlap values, and caused reordering of some modes.

https://doi.org/10.1021/acsomega.4c00523
ACS Omega 2024, 9, 24520−24537

Interestingly, the perturbations observed in the Ser20 phosphorylated protein (Figure 6A, right) were not necessarily mirrored in the Thr12 phosphorylated protein, underscoring phosphorylated residue-specific effects (Figure 6B, right). For instance, the low-frequency global motions associated with mode 10 of the unphosphorylated form were manifested in mode 7 for Ser20 phosphorylated polyubiquitin but were largely retained in the same mode for the Thr12 phosphorylated protein. Similarly, mode 1 motions of the unphosphorylated protein were reordered to mode 2 in the Thr12 phosphorylated state but were lost in the Ser20 phosphorylated form. The evaluation of Cα-deviation patterns in both Ser20 (Figure 6C,i) and Thr12 (Figure 6C,ii) phosphorylated proteins compared to the unphosphorylated form unveiled distinct behaviors. While both phosphorylated forms exhibited significant deviation in the β1-β2 loop, the Thr12 phosphorylated form displayed additional significant deviations in regions such as the C-α1, α2, β3, β3-β4 loop, and β4. Examining the lysine residues crucial for forming isopeptide bonds revealed differing degrees of deviations in both Ser20 and Thr12 phosphorylated forms, emphasizing phosphorylated residue-specific impacts on polyubiquitin chain formation and protein functionality. The patterns of the fluctuation difference for Ser20 (Figure 6D,i) and Thr12 (Figure 6D,ii) phosphorylation proteins compared to the unphosphorylated form were found to be different for each phosphorylated protein. Once again, the β1-β2 region showed significant differences in fluctuation in both cases. In the Ser20 phosphorylated case, the β3-β4 loop also showed a significant fluctuation difference, but this was not observed in the Thr12 phosphorylated protein. Significance was attributed only if the difference exceeded the standard deviation from the mean of the fluctuation difference in the control data set. Furthermore, investigating the global motions for mode 9 of both phosphorylated forms, the unphosphorylated form revealed nuanced differences (Figure 6E and Supplementary Movie 1). Mode 9 was chosen for analysis due to its moderate overlap with the unphosphorylated form in Thr12 phosphorylation and low overlap in Ser20 phosphorylation. This allowed us to compare the low-frequency global motion seen in the unphosphorylated form, which was not retained in the Ser20 phosphorylated form but was marginally preserved in the Thr12 phosphorylated form. Notably, the β1-β2 loop consistently exhibited significant fluctuations in both phosphorylated forms compared to the unphosphorylated form, with greater magnitudes in the phosphorylated states. In the Ser20 phosphorylated case, significant differences in the fluctuations of the β3-β4 loop were observed compared with the unphosphorylated protein, a feature less pronounced in the Thr12 phosphorylated case (as visualized by the length of eigenvectors). Additionally, we performed a phosphonull mutation on Ser20 phosphorylated polyubiquitin B mutating the phosphorylated residue to alanine (Supplementary Figure 6). We observed alterations in the conformational dynamics of the β3-β4 loop, situated distal from the phosphorylation site. Initially, significant fluctuations in this region became nonsignificant upon phosphonull mutation, suggesting a dampening effect. Moreover, we observed a decrease in the magnitude of fluctuations for the β1-β2 loop (Supplementary Figure 6A). Furthermore, a majority of low-frequency modes, previously perturbed by phosphorylation, lost and associated with new low-frequency motions, exhibited increased retention upon phosphonull mutation, as indicated by higher overlap values (Supplementary Figure 6B). These findings underscore the intricate role of phosphorylation in orchestrating delicate conformational dynamics, which is crucial for protein function. Disruption of this balance by phosphonull mutations highlights the regulatory significance of phosphorylation in governing protein behavior. Moreover, no notable alterations were observed in the total accessible surface area following Ser 20 phosphorylation in polyubiquitin B.

Overall, this case study highlights that the type and position of the phosphorylated residue intricately influence the structural dynamics of polyubiquitin B, potentially leading to divergent functional outcomes. The observed variations in global modes, local structural deviations, and fluctuations provide valuable insights into the residue-specific impact of phosphorylation on the structural and dynamic properties of polyubiquitin B.

Phosphorylation within a Kinase's Activation Loop Brings About Functional Changes by Influencing Its Structure and Dynamics: A Case Study on Glycogen Synthase Kinase-3 Beta. Glycogen synthase kinase-3 beta (GSK-3β) is a serine/threonine protein kinase that plays a crucial role in various cellular processes including glycogen metabolism, cell proliferation, differentiation, and apoptosis. One important aspect of GSK-3β regulation is its phosphorylation at Tyr216, which activates the kinase. This phosphorylation event is often associated with an increased GSK-3β activity. Activated GSK-3β, in turn, phosphorylates a range of substrate proteins, exerting regulatory control over diverse cellular functions.[24,25] The phosphorylation of GSK-3β at tyrosine 216 has been implicated in several biological processes. For instance, it has been shown to be involved in mechanisms of neuronal survival.[26] Additionally, the phosphorylation of GSK-3β at tyrosine 216 has been linked to the regulation of tau protein, which is associated with neurodegenerative diseases like Alzheimer's disease.[27,28] An abnormal GSK-3β activity can contribute to pathological processes associated with these diseases. A comprehensive understanding of the role of GSK-3β in cellular signaling necessitates a detailed exploration of its phosphorylation patterns.

We conducted a comparative conformational analysis of GSK-3β in its Tyr216 phosphorylated and unphosphorylated forms. The two forms exhibited a Cα-RMSD of 1.62 Å, highlighting substantial structural disparities (Figure 7A). A detailed examination of the aligned residues revealed significant backbone deviations in the N-terminal lobe, particularly the β3-αC loop and specific regions of the C-terminal lobe (Figure 7B). The β3-αC loop plays a crucial role in kinase activation. This loop facilitates the movement of the C-lobe, which is essential for maintaining kinase activity.[29] The observed structural changes in this loop are integral to kinase activation, ensuring that the kinase remains functional and capable of carrying out its cellular functions effectively. Furthermore, the N-terminal lobe displayed a higher difference in flexibility, particularly in the glycine-rich loop compared to the C-terminal lobe. This observation aligns with the characteristic motions observed in active kinases (Figure 7C). Importantly, the regions exhibiting significant flexibility were found to be distant from the phosphorylation site, suggesting long-range dynamic changes resulting from phosphorylation. Additionally, we investigated the preservation of low-frequency global modes and found that only a limited subset of modes was preserved post-phosphorylation, with a majority being lost and a few modes undergoing reordering (Figure 7D). A focused investigation into mode 5 motions demonstrated distinct differences between the two forms. The phosphorylated kinase exhibited characteristic lobe opening and closing motions, reminiscent of active kinases, a

https://doi.org/10.1021/acsomega.4c00523
ACS Omega 2024, 9, 24520−24537

motion absent in the unphosphorylated form. Moreover, the β3-αC loop in the unphosphorylated form displayed substantial fluctuations, contributing to significant differences in fluctuation dynamics in this region (Figure 7E and Supplementary Movie 2). Our findings highlight substantial conformational disparities between the phosphorylated and unphosphorylated forms of GSK-3β, revealing specific structural and dynamic alterations induced by phosphorylation including long-range effects and alterations in low-frequency global modes. Additionally, following Tyr216 phosphorylation in GSK-3β, a noticeable decrease in the overall accessible surface area (ASA) is observed, accompanied by a reduction in the percentage of exposed residues and an increase in the number of buried residues. The most striking alteration is observed in phosphosite (Str), where the total ASA decreases, with a modest decline in the ASA in the away from phosphosite (Str) region. However, notably distinctively, in the near-phosphosite (Str) region, there is an increase in the total ASA following phosphorylation.

DISCUSSION

Our study explores an intricate landscape of phosphorylation-induced conformational dynamics, providing a detailed investigation of the alterations in protein structure, dynamics, and surface accessibility. The nuanced findings shed light on the multifaceted impact of single-site phosphorylation, uncovering both local and global effects that contribute to the regulatory tapestry of cellular processes. One of the key observations from our study is the distinctive conformational changes that proteins undergo upon phosphorylation. The structural alterations extend far beyond the phosphorylation site, with more pronounced changes occurring distally. This emphasizes the ripple effect of phosphorylation on the protein structure, indicating a sophisticated network of conformational adjustments that intricately shape the functional properties of proteins. For our exploration of phosphorylation-induced dynamic shifts in protein residues through normal mode analysis (NMA), we provided nuanced insights into alterations in vibrational modes and flexibility. The observed significant differences in normalized square fluctuations between phosphorylated and unphosphorylated forms indicate a post-phosphorylation augmentation in the dynamic motion of residues. The robustness of these findings was confirmed through consistent observations across different distance cutoffs, reinforcing the reliability of our results. Contrary to the dynamic shifts observed, the residue motion correlation remained largely stable post-phosphorylation, indicating robustness in the local interactions and coordinated movements between residues. However, an intricate duality emerged when exploring low-frequency global modes. The low overlap observed in a majority of cases suggests a substantial shift in the mode preference and order upon phosphorylation. This emphasizes that while local interactions may persist, the larger-scale, global modes of motion are distinctly influenced by phosphorylation, showcasing a nuanced alteration in the collective dynamics of the protein. The investigation into the total accessible surface area (ASA) post-phosphorylation revealed diverse effects on protein exposure and interaction capabilities. A substantial portion of proteins exhibited changes in the total ASA, with some showcasing an increase and others showcasing a reduction. The region-specific differences, especially in the near-phosphosite (Str) category, underscore the localized impact of phosphorylation on creating more exposed surfaces in proximity to phosphorylation sites. The case study on polyubiquitin B offers gripping insight into the residue-specific phosphorylation effects on the structural dynamics, providing a nuanced understanding of the molecular mechanisms underlying its functionality. Our analysis reveals that phosphorylation induces significant alterations in global modes, with distinct differences observed between the Ser20 and Thr12 phosphorylated forms. Moreover, specific regions, such as the β1-β2 loop and β3-β4 loop, exhibit notable, yet differential structural deviations and fluctuations, underscoring the residue-specific impacts of phosphorylation on protein dynamics. These findings emphasize the nuanced effects of phosphorylation at different residues and highlight the importance of considering residue specificity in understanding the regulatory mechanisms of protein function. This case underscores the need for future research to unravel the distinct functional implications of phosphorylation on different residues and at different locations, contributing to a more comprehensive understanding of residue-position specificity and further elucidating the role of phosphorylation in governing cellular processes. The case study on glycogen synthase kinase-3 beta (GSK-3β) provides a detailed exploration of how phosphorylation within the activation loop at Tyr216 influences the structure and dynamics of the kinase, thereby impacting its functionality in various cellular processes. Our comparative conformational analysis of GSK-3β in its Tyr216 phosphorylated and unphosphorylated forms revealed substantial structural disparities, with a Cα-RMSD of 1.62 Å between the two forms. Specifically, significant backbone deviations were observed in the N-terminal lobe, particularly in the β3-αC loop and specific regions of the C-terminal lobe, which are crucial for kinase activation. Moreover, the N-terminal lobe displayed higher flexibility, particularly in the glycine-rich loop, compared with the C-terminal lobe, aligning with characteristic motions observed in active kinases. The long-range effects, preservation of specific global modes, and residue-specific fluctuation dynamics underscore the intricate relationship between phosphorylation and kinase activity. Future research endeavors can build upon these findings, further elucidating the molecular mechanisms that govern GSK-3β regulation and its implications for cellular processes and disease pathology. Moreover, we also recognize the importance of investigating multiple phosphorylation events, as they can synergistically influence protein behavior. For this, we analyzed dual-site phosphorylation in tyrosine protein kinase JAK2, specifically targeting consecutive tyrosine residues 1007 and 1008. Our analysis revealed significant structural deviations in both N- and C-terminal domains (Supplementary Figure 5A), along with notable alterations in fluctuations in specific regions, located distal to the phosphorylated residue, within these domains (Supplementary Figure 5B). Importantly, we observed consistent patterns in intraresidue cross-correlations, indicating that the coupling between residue fluctuations remained largely unaffected post-phosphorylation (Supplementary Figure 5C). While it would have been ideal to explore instances where proteins are crystallized in single, double, triple, and unphosphorylated forms to examine the gradual effects of phosphate moieties, such cases were not readily available in the Protein Data Bank. Nonetheless, we emphasize that each type of phosphorylation, coupled with its distinct location on amino acid residues and the surrounding microenvironment, carries specific implications for protein structure, function, and cellular signaling.

Furthermore, we opted for all-atom NMA using Bio3d[30] to validate whether the trends observed in anisotropic network

https://doi.org/10.1021/acsomega.4c00523
ACS Omega 2024, 9, 24520−24537

model (ANM)-normal mode analysis (NMA) at a coarse-grained Cα atom level hold true at the all-atom level (Supplementary Figure 7). Notably, both of these techniques, ANM-NMA and all-atom NMA, yielded similar conformational changes for both polyubiquitin B (Supplementary Figure 7A) and glycogen synthase kinase-3 beta (Supplementary Figure 7B). This consistency between coarse-grained ANM-NMA and all-atom NMA lends robustness to our findings, suggesting that the observed conformational changes are not artifacts of the modeling approach but rather inherent features of the system under investigation. Therefore, despite the differences in resolution and computational methodologies between ANM-NMA and all-atom NMA, their agreement reinforces the validity and reliability of our conclusions. A recent study analyzed protein structural changes within neighborhoods of 3−15 amino acid residues from phosphorylation sites, focusing on alterations in geometric parameters such as the radius of gyration (R_g), RMSD, Cα displacement, and SASA.[31] What sets our study apart is its systematic approach to comprehensively exploring the impact of single-site phosphorylation on protein structure and dynamics. We employ stringent filtration criteria applied to the data set to ensure robustness and reliability in the observations. By meticulously curating the SSP data set, we guarantee that any observed differences between phosphorylated and unphosphorylated forms are solely attributed to the addition of a phosphate moiety, thereby eliminating confounding variables. Furthermore, our study incorporates a control data set against which observations are meticulously compared to ascertain significance. This control data set serves as a crucial benchmark, facilitating a thorough evaluation of the structural and dynamic changes induced by phosphorylation. Additionally, categorizing residues based on their proximity to the phosphorylation site, into phosphosite (Seq), non-phosphosite (Seq), phosphosite (Str), near-phosphosite (Str), and away from phosphosite (Str) residues, allows for a granular analysis of conformational alterations linked to the phosphorylation event. Such systematic categorization enables the identification of both local and global effects of phosphorylation on the protein structure and dynamics. Moreover, our study goes beyond merely examining topical changes in the protein structure. We delve into dynamic shifts in protein residues, emphasizing the long-range impact of phosphorylation on the protein dynamics. This includes investigating how phosphorylation affects the residue motion correlation and perturbs low-frequency global modes in the unphosphorylated form. By incorporating such dynamic analyses, we provide a comprehensive understanding of the multifaceted effects of phosphorylation on protein behavior. Overall, our study's rigorous methodology, systematic approach to data set selection, stringent filtration criteria, categorization of residues, and dynamic analyses collectively contribute to a thorough investigation of phosphorylation-induced conformational dynamics. A primary limitation of our research is the availability of suitable crystal structures in both phosphorylated and unphosphorylated forms in the Protein Data Bank (PDB). The stringent filtering criteria applied, necessitated by the nature of our study, further reduced the number of eligible protein pairs. This dual constraint, stemming first from the limited availability of relevant structures and then from our rigorous filtration process, restricted the size and diversity of our data set. Consequently, the outcomes and generalizability of our findings may be influenced by this inherent limitation in the selection of proteins for analysis. Despite these constraints, our study provides valuable insights into the structural and dynamic effects of protein phosphorylation, paving the way for future investigations with an expanded and more diverse data set.

In conclusion, our study provides valuable insights into the conformational, dynamics, and surface accessibility alterations induced by phosphorylation. By elucidating the intricacies of phosphorylation-induced structure-dynamics-accessibility changes, we contribute to a more comprehensive understanding of the regulatory mechanisms underlying cellular processes. This knowledge can pave the way for the development of targeted therapeutic strategies aimed at modulating phosphorylation events and their associated cellular signaling networks.

MATERIALS AND METHODS

Data Set Preparation. *SSP Data Set for Structural Comparison.* Each pair consisted of both phosphorylated (in serine/threonine or tyrosine, denoted as SEP/TPO/PTR) and unphosphorylated forms. The data curation process involved applying stringent filtering conditions:

1. All protein pairs must have 3D crystal structures available in both phosphorylated and unphosphorylated states, with no missing residues at or near the phosphorylated residue.
2. The resolution of the structures should be better than 3 Å.
3. Both phosphorylated and unphosphorylated forms must share the same UniProt identifier.
4. The oligomeric state of both the forms should be identical (here, AU = 1, BA = 1), as determined by examining PDB biological unit information.
5. Both forms should either have similar ligands or no ligands bound. This condition was imposed to minimize and mitigate biases arising due to the presence of ligands.
6. Exclusion of proteins with disordered regions.
7. Both phosphorylated and unphosphorylated forms should either have no mutation or identical mutations.
8. The phosphate moiety should be present as a modified residue, distinct from the classification as a ligand.

These rigorous criteria were implemented to ensure that any observed differences between the phosphorylated and unphosphorylated forms are solely attributed to the addition of a phosphate moiety.

SSP Data Set for Dynamics Analysis. To understand the nuanced dynamics and flexibility changes within protein structures upon phosphorylation, the initial data set underwent additional refinement. Instances with missing residues in either the phosphorylated or unphosphorylated state were excluded. Enforcement of this filtering condition aimed to preclude potential bias stemming from the necessity of modeling missing regions in the protein structure. Consequently, 17 protein pairs, totaling 34 distinct protein structures, satisfying the refined criteria were identified and selected for subsequent analyses.

Control Data Set. The control group consisted of phosphorylated protein structures from representative protein pairs in the SSP data set, resolved under varied crystallographic conditions. These structures were further filtered to ensure the presence of single chains in both the asymmetric unit (AU) and biological assembly (BA), to maintain congruence with the oligomeric state of protein pairs in the SSP data set. Care was taken to ascertain the absence of additional biological entities, such as peptides, RNA, or DNA, in both the AU and BA. Further refinement involved applying a resolution cutoff of 3 Å and exclusion of structures with missing residues. A refined subset comprising 98 structures was thus identified and selected as the

https://doi.org/10.1021/acsomega.4c00523
ACS Omega 2024, 9, 24520−24537

control for subsequent analyses. This carefully curated control data set serves as a reference to elucidate the impact of crystal packing on protein conformation. Importantly, it serves as a baseline, representing background noise against which significant differences between phosphorylated and unphosphorylated forms can be discerned and quantified.

Estimating the Likelihood of Phosphorylated Residue Occurrence within Secondary Structures. The propensity of a phosphate moiety occurring in helices, β-strands, or loops within the SSP data set was determined using the following formula:

$$\text{propensity of the phosphorylated residue to occur in X (SSP data set)} = \left(\frac{\text{number of phosphorylated residues in X}}{\text{total number of phosphorylation residues}}\right) \Big/ \left(\frac{\text{number of residues in X}}{\text{total number of residues}}\right)$$

where X is helices/β-sheets/loops.

Classification of Localized Regions by Integrating Sequence and Structural Perspectives. In this study, protein residues were classified into distinct categories based on two key criteria: sequence and structural proximity.

Sequence-Based Classification. The sequence-centric approach involved categorization of protein residues into two groups: "phosphosite" and "non-phosphosite". Phosphosite (Seq) is defined as heptapeptides spanning from P-3 to P+3, with the "P" representing the phosphorylated residue, while non-phosphosite (Seq) includes all residues outside this heptapeptide range. This heptapeptide motif, with the phosphorylated residue at the central position (P) and surrounding residues labeled as P-3 to P+3, is chosen due to its extensive use in the literature for kinase substrate identification.[32,33] This motif aligns with kinase recognition specificity, making it a valuable starting point in the study of phosphorylation events.

Structural Proximity Classification. The structural classification zooms in on spatial relationships, further dividing localized regions into "phosphosite", "near-phosphosite", and "away from phosphosite" based on proximity to the phosphorylated residue, employing specific distance criteria. Phosphosite (Str) includes residues within a 4.5 Å proximity, determined by an interatomic distance cutoff. The near-phosphosite (Str) category encompasses residues situated more than 4.5 Å but less than 10 Å away, while the away from phosphosite (Str) group includes residues positioned more than 10 Å from the phosphorylated residue.

Structural Analyses. The TM-align method was employed to align the structures of phosphorylated and unphosphorylated forms within each protein pair. TM-align, a widely recognized structural alignment algorithm in bioinformatics, facilitates the comparison and alignment of protein structures by emphasizing both sequential and spatial information.[34] The algorithm proves to be particularly useful for comparing proteins with similar overall folds but potentially different local conformations, a scenario often encountered in studies involving phosphorylated and unphosphorylated forms of proteins.

Following the structural alignment, the backbone root-mean-square deviation (RMSD) was computed as a metric to quantify the dissimilarity between the aligned structures. RMSD is a measure of the average distance between the corresponding atoms in two structures. Mathematically, the RMSD between two sets of coordinates $(X1, Y1, Z1)$ and $(X2, Y2, Z2)$ for a set of atoms is calculated as follows:

$$\text{RMSD} = \sqrt{\frac{\sum_{i=1}^{N}((X1_i - X2_i)^2 + (Y1_i - Y2_i)^2 + (Z1_i - Z2_i)^2)}{N}}$$

Here, N represents the number of atoms considered in the calculation. A higher RMSD value indicates lower structural similarity, with values exceeding the standard deviation from the mean of RMSDs in the control data set being considered as statistically significant differences. Additionally, we computed the TM-score, which provides a complementary assessment of the structural similarity.

To compute local structural variations, individual α-carbon (Cα)-deviations between equivalent residue positions in both phosphorylated and unphosphorylated forms were calculated. The RMSD between phosphorylated and unphosphorylated proteins was computed for specific regions, including phosphosite (Seq), non-phosphosite (Seq), phosphosite (Str), near-phosphosite (Str), and away from phosphosite (Str). These analyses were conducted for each protein pair in the SSP data set, providing a comprehensive understanding of localized structural deviations in relation to phosphorylation states.

Coarse-Grained Dynamics Analysis (Utilizing Normal Mode Analysis with ANM). Understanding long-time scale protein motions is crucial in deciphering their functional significance, and normal mode analysis (NMA) stands out as a preferred method for such investigations.[35−37] NMA relies on a set of Cartesian coordinates derived from the protein structure and a force field defining interatomic interactions. The process involves generating a "Hessian" matrix from the second derivative of potential energy followed by diagonalization to yield eigenvalues and eigenvectors.

Previous studies have demonstrated that global protein motions, characterized by low-frequency collective movements, play a pivotal role in signifying biologically relevant functions.[36,38] The computational challenge posed by all-atom NMA, given its extensive calculations, led us to adopt a coarse-grained approach using the Cα-level anisotropic network model (ANM)-based NMA for this study.[39] The choice of Cα-level NMA was grounded in its ability to successfully corroborate with both experimental and molecular dynamics data, providing insights into dynamics over extended timescales.[40,41]

The calculations pertaining to normal mode analyses were executed using the ProDy package.[42] Normal modes were computed for 17 protein pairs in both phosphorylated and unphosphorylated forms, resulting in a total of 34 (17 × 2) calculations, alongside a control data set.

For the coarse-grained model, Cα atoms, represented as masses, were connected by elastic springs with identical spring constants if their inter-Cα distance was less than 15 Å, with variations tested using 12 and 10 Å cutoffs. Exclusion of contributions from three N-terminal and three C-terminal residues was implemented. Mean-squared fluctuations were scaled using z-score normalization, and significance in the differences between normalized square fluctuations of phosphorylated and unphosphorylated forms was determined by comparing them to the standard deviation from the mean of differences in the control data set. This analysis was conducted for the entire protein and specific regions, including phosphosite (Seq), non-phosphosite (Seq), phosphosite (Str), near-phosphosite (Str), and away from phosphosite (Str). To quantify dynamics, the root-mean-squared difference of fluctuations (RMSDf) was computed as an equivalent of

https://doi.org/10.1021/acsomega.4c00523
ACS Omega 2024, 9, 24520−24537

RMSD, involving the difference between normalized fluctuations of phosphorylated and unphosphorylated forms.

Cross-correlation, indicating the correlation between fluctuations, was computed for all of the structures. The R_v coefficient, a multivariate generalization of Pearson's coefficient, was employed to quantify the similarity between cross-correlation matrices.[43] Furthermore, to gauge the accessibility of intrinsic motions in the phosphorylated form to the unphosphorylated form, the overlap, representing the inner product of eigenvectors from the 10 lowest frequency modes, was calculated using the ProDy package.[44,45] This provided insight into the extent of shared conformational space between the two forms, shedding light on the protein's dynamical behavior.

Solvent Accessibility Analyses. Solvent accessibility refers to the degree to which a residue is exposed to or buried within the protein structure. Solvent accessibility analyses play a crucial role in understanding the structural characteristics of proteins.[46] In this study, a specialized tool NetPhos 3.1 was employed to assess the solvent accessibility of proteins in the SSP data set. NetPhos 3.1 is a machine learning model that has been trained on a diverse data set of experimentally verified phosphorylation events.[47]

To determine the solvent accessibility of specific residues, NetPhos 3.1 utilizes a sequence-based method. It distinguishes between exposed and buried residues by applying a threshold of 25% of the relative accessible surface area (RASA). NetPhos 3.1 was chosen for computing solvent accessibility in phosphorylated proteins due to its specialized training on experimental phosphorylation cases, enabling accurate prediction of solvent accessibility for phosphorylated residues and offering insights into their functional and structural implications.

To assess the impact of phosphorylation, we calculated the total accessible surface area (ASA) for both phosphorylated and unphosphorylated forms of the proteins. Equivalent residues in both states were taken into consideration during the analysis. Furthermore, we computed the total accessible surface area for specific regions, including the phosphosite (Seq), non-phosphosite (Seq), phosphosite (Str), near-phosphosite (Str), and away from phosphosite (Str) regions, for each protein pair in the SSP data set.

To quantify the change in solvent accessibility, we calculated the percentage change in the total accessible surface area as follows:

$$\begin{aligned}&\text{percentage change}_{\text{region-of-interest}}\\&= \left[\left(\text{total ASA}_{\text{phosphorylated-protein-specific-region}}\right.\right.\\&\left.\left. - \text{total ASA}_{\text{unphosphorylated-protein-specific-region}}\right) \times 100\right]\\&/\left[\text{total ASA}_{\text{unphosphorylated-protein-specific-region}}\right]\end{aligned}$$

Statistical Analyses. Statistical significance was assessed using both the 2-sample Kolmogorov–Smirnov (KS) test and the *t* test to scrutinize the distributional disparities between two groups: phosphorylated proteins and unphosphorylated proteins in the SSP data set. All statistical analyses were carried out in the Python programming environment.

Visualization. UCSF Chimera[48] was used for protein structure visualization, and ".nmd" extension files created using ProDy were used to explore normal modes in Visual Molecular Dynamics (VMD)[49] with the help of the NMWiz (Normal Mode Wizard) plugin. For comparative assessments of normal modes, informative videos were produced by using the MovieMaker plugin in VMD, complemented by VideoMach.

■ ASSOCIATED CONTENT

Supporting Information

The Supporting Information is available free of charge at https://pubs.acs.org/doi/10.1021/acsomega.4c00523.

Table with detailed information for protein pairs in the SSP data set, including UniProt ID, PDB ID, protein name, modified residue, and resolution; workflow for SSP data set curation and modified residue localization in phosphorylated proteins; structural insights into the SSP data set; normal mode fluctuation calculation at 12 and 10 Å cutoffs; dynamic/flexibility alterations in the SSP data set; impact of dual tyrosine phosphorylation on tyrosine protein kinase JAK2; effect of phosphonull mutation on Ser20 phosphorylated polyubiquitin B; changes in flexibility post-phosphorylation (PDF)

Supplementary movie on case studies: distinct large-scale Cα-backbone fluctuations in polyubiquitin B (MP4)

Supplementary movie on case studies: distinct large-scale Cα-backbone fluctuations in glycogen synthase kinase-3 beta (MP4)

■ AUTHOR INFORMATION

Corresponding Author

Ramanathan Sowdhamini − *Molecular Biophysics Unit, Indian Institute of Science, Bangalore 560012, India; Computational Approaches to Protein Science, National Centre for Biological Sciences, Bangalore 560065, India; Computational Biology, Institute of Bioinformatics and Applied Biotechnology, Bangalore 560100, India;* orcid.org/0000-0002-6642-2367; Email: mini@ncbs.res.in

Authors

Seemadri Subhadarshini − *Molecular Biophysics Unit, Indian Institute of Science, Bangalore 560012, India*

Himani Tandon − *Molecular Biophysics Unit, Indian Institute of Science, Bangalore 560012, India*

Narayanaswamy Srinivasan − *Molecular Biophysics Unit, Indian Institute of Science, Bangalore 560012, India*

Complete contact information is available at: https://pubs.acs.org/10.1021/acsomega.4c00523

Author Contributions

S.S. conducted research, analyzed data, and prepared the initial draft of the manuscript. N.S. conceptualized the project and provided supervision. H.T. also provided supervision for the project and reviewed the first draft. R.S. administered the project, secured research funding, and reviewed the manuscript.

Notes

The authors declare no competing financial interest.

■ ACKNOWLEDGMENTS

R.S. acknowledges funding and support provided by the JC Bose Fellowship (JBR/2021/000006) from the Science and Engineering Research Board, India and the Bioinformatics Centre Grant funded by the Department of Biotechnology, India (BT/PR40187/BTIS/137/9/2021). R.S. would also like to thank the Institute of Bioinformatics and Applied Biotechnology for the funding through her Mazumdar-Shaw Chair in Computational Biology (IBAB/MSCB/182/2022). S.S. is supported by PMRF

(Prime Ministers' Research Fellowship) awarded by the Government of India.

DEDICATION

This article is dedicated to the memory of late Prof. Narayanaswamy Srinivasan.

REFERENCES

(1) Garcia-Garcia, T.; Poncet, S.; Derouiche, A.; Shi, L.; Mijakovic, I.; Noirot-Gros, M.-F. Role of Protein Phosphorylation in the Regulation of Cell Cycle and DNA-Related Processes in Bacteria. *Front. Microbiol.* **2016**, *7*, 184.
(2) Mayr, B.; Montminy, M. Transcriptional regulation by the phosphorylation-dependent factor CREB. *Nat. Rev. Mol. Cell Biol.* **2001**, *2*, 599−609.
(3) Ardito, F.; Giuliani, M.; Perrone, D.; Troiano, G.; Lo Muzio, L. The crucial role of protein phosphorylation in cell signaling and its use as targeted therapy (Review). *Int. J. Mol. Med.* **2017**, *40*, 271−280.
(4) Wang, J. P.; Chuang, L.; Loziuk, P. L.; Chen, H.; Lin, Y.-C.; Shi, R.; et al. Phosphorylation is an on/off switch for 5-hydroxyconiferaldehyde *O* -methyltransferase activity in poplar monolignol biosynthesis. *Proceedings of the National Academy of Sciences.* **2015**, *112*, 8481−6.
(5) Oeckinghaus, A.; Ghosh, S. The NF- B Family of Transcription Factors and Its Regulation. *Cold Spring Harb Perspect Biol.* **2009**, *1*, a000034−a000034.
(6) ZHANG, W.; LIU, H. T. MAPK signal pathways in the regulation of cell proliferation in mammalian cells. *Cell Res.* **2002**, *12*, 9−18.
(7) Solaro, R. J.; Henze, M.; Kobayashi, T. Integration of Troponin I Phosphorylation With Cardiac Regulatory Networks. *Circ. Res.* **2013**, *112*, 355−66.
(8) Tsai, C.-J.; del Sol, A.; Nussinov, R. Protein allostery, signal transmission and dynamics: a classification scheme of allosteric mechanisms. *Mol. Biosyst.* **2009**, *5*, 207.
(9) Tandon, H.; de Brevern, A. G.; Srinivasan, N. Transient association between proteins elicits alteration of dynamics at sites far away from interfaces. *Structure* **2021**, *29*, 371−384.e3.
(10) Seok, S.-H. Structural Insights into Protein Regulation by Phosphorylation and Substrate Recognition of Protein Kinases/Phosphatases. *Life.* **2021**, *11*, 957.
(11) Mahita, J.; Sowdhamini, R. Probing subtle conformational changes induced by phosphorylation and point mutations in the TIR domains of TLR2 and TLR3. *Proteins: Struct., Funct., Bioinf.* **2018**, *86*, 524−535.
(12) Hughes, C. A.; Mandell, J. G.; Anand, G. S.; Stock, A. M.; Komives, E. A. Phosphorylation causes subtle changes in solvent accessibility at the interdomain interface of methylesterase CheB. *J. Mol. Biol.* **2001**, *307*, 967−76. 1 1Edited by P. E. Wright.
(13) Paul, A.; Subhadarshini, S.; Srinivasan, N. Pseudokinases repurpose flexibility signatures associated with the protein kinase fold for noncatalytic roles. *Proteins: Structure, Function, and Bioinformatics.* **2022**, *90*, 747−64.
(14) Wako, H.; Endo, S. Normal mode analysis as a method to derive protein dynamics information from the Protein Data Bank. *Biophys Rev.* **2017**, *9*, 877−93.
(15) Bahar, I.; Lezon, T. R.; Bakan, A.; Shrivastava, I. H. Normal Mode Analysis of Biomolecular Structures: Functional Mechanisms of Membrane Proteins. *Chem. Rev.* **2010**, *110*, 1463−97.
(16) Kumar, A.; Mandiyan, V.; Suzuki, Y.; Zhang, C.; Rice, J.; Tsai, J.; et al. Crystal Structures of Proto-oncogene Kinase Pim1: A Target of Aberrant Somatic Hypermutations in Diffuse Large Cell Lymphoma. *J. Mol. Biol.* **2005**, *348*, 183−93.
(17) Ose, N. J.; Butler, B. M.; Kumar, A.; Kazan, I. C.; Sanderford, M.; Kumar, S.; et al. Dynamic coupling of residues within proteins as a mechanistic foundation of many enigmatic pathogenic missense variants. *PLoS Comput. Biol.* **2022**, *18*, No. e1010006.
(18) Marcos, E.; Crehuet, R.; Bahar, I. Changes in Dynamics upon Oligomerization Regulate Substrate Binding and Allostery in Amino Acid Kinase Family Members. *PLoS Comput. Biol.* **2011**, *7*, No. e1002201.
(19) Oliwa, T.; Shen, Y. cNMA: a framework of encounter complex-based normal mode analysis to model conformational changes in protein interactions. *Bioinformatics.* **2015**, *31*, i151−60.
(20) Morimoto, D.; Shirakawa, M. The evolving world of ubiquitin: transformed polyubiquitin chains. *Biomol Concepts.* **2016**, *7*, 157−67.
(21) Yu, Y.; Zheng, Q.; Erramilli, S. K.; Pan, M.; Park, S.; Xie, Y.; et al. K29-linked ubiquitin signaling regulates proteotoxic stress response and cell cycle. *Nat. Chem. Biol.* **2021**, *17*, 896−905.
(22) Kazlauskaite, A.; Kondapalli, C.; Gourlay, R.; Campbell, D. G.; Ritorto, M. S.; Hofmann, K.; et al. Parkin is activated by PINK1-dependent phosphorylation of ubiquitin at Ser65. *Biochem. J.* **2014**, *460*, 127−41.
(23) Wauer, T.; Swatek, K. N.; Wagstaff, J. L.; Gladkova, C.; Pruneda, J. N.; Michel, M. A.; et al. Ubiquitin Ser65 phosphorylation affects ubiquitin structure, chain assembly and hydrolysis. *EMBO J.* **2015**, *34*, 307−25.
(24) Takahashi-Yanaga, F.; Shiraishi, F.; Hirata, M.; Miwa, Y.; Morimoto, S.; Sasaguri, T. Glycogen synthase kinase-3β is tyrosine-phosphorylated by MEK1 in human skin fibroblasts. *Biochem. Biophys. Res. Commun.* **2004**, *316*, 411−5.
(25) Hughes, K.; Nikolakaki, E.; Plyte, S. E.; Totty, N. F.; Woodgett, J. R. Modulation of the glycogen synthase kinase-3 family by tyrosine phosphorylation. *EMBO J.* **1993**, *12*, 803−8.
(26) Maixner, D. W.; Weng, H.-R. The Role of Glycogen Synthase Kinase 3 Beta in Neuroinflammation and Pain. *J. Pharm. Pharmacol.* **2013**, *1*, No. 001.
(27) Hanger, D. P.; Noble, W. Functional Implications of Glycogen Synthase Kinase-3-Mediated Tau Phosphorylation. *Int. J. Alzheimers Dis.* **2011**, *2011*, 1−11.
(28) Lauretti, E.; Dincer, O.; Praticò, D. Glycogen synthase kinase-3 signaling in Alzheimer's disease. Biochimica et Biophysica Acta (BBA) - Molecular. *Cell Research.* **2020**, *1867*, No. 118664.
(29) Jani, V.; Sonavane, U.; Sawant, S. Structural insights into the activation mechanism of phosphoinositide 3-kinase alpha. *Comput. Biol. Chem.* **2024**, *108*, No. 107994.
(30) Grant, B. J.; Skjærven, L.; Yao, X. Q. The Bio3D packages for structural bioinformatics. *Protein Sci.* **2021**, *30*, 20.
(31) Nikolsky, K. S.; Kulikova, L. I.; Petrovskiy, D. V.; Rudnev, V. R.; Malsagova, K. A.; Kaysheva, A. L. Analysis of Structural Changes in the Protein near the Phosphorylation Site. *Biomolecules* **2023**, *13*, 1564.
(32) Saunders, N. F. W.; Brinkworth, R. I.; Kemp, B. E.; Kobe, B.Substrates of Cyclic Nucleotide-Dependent Protein Kinases. In: *Handbook of Cell Signaling.* Elsevier; 2010. p 1489−95.
(33) Dennis, E. A.; Bradshaw, R. A.*Transduction mechanisms in cellular signaling: Cell signaling collection*. 1st ed. Academic Press; 2011.
(34) Zhang, Y. TM-align: a protein structure alignment algorithm based on the TM-score. *Nucleic Acids Res.* **2005**, *33*, 2302−9.
(35) Go, N.; Noguti, T.; Nishikawa, T. Dynamics of a small globular protein in terms of low-frequency vibrational modes. *Proceedings of the National Academy of Sciences.* **1983**, *80*, 3696−700.
(36) Brooks, B.; Karplus, M. Harmonic dynamics of proteins: normal modes and fluctuations in bovine pancreatic trypsin inhibitor. *Proceedings of the National Academy of Sciences.* **1983**, *80*, 6571−5.
(37) Bahar, I.; Rader, A. Coarse-grained normal mode analysis in structural biology. *Curr. Opin Struct Biol.* **2005**, *15*, 586−92.
(38) Bahar, I.; Lezon, T. R.; Yang, L.-W.; Eyal, E. Global Dynamics of Proteins: Bridging Between Structure and Function. *Annu. Rev. Biophys.* **2010**, *39*, 23−42.
(39) Tirion, M. M. Large Amplitude Elastic Motions in Proteins from a Single-Parameter, Atomic Analysis. *Phys. Rev. Lett.* **1996**, *77*, 1905−8.
(40) Valadié, H.; Lacapčre, J. J.; Sanejouand, Y.-H.; Etchebest, C. Dynamical Properties of the MscL of Escherichia coli: A Normal Mode Analysis. *J. Mol. Biol.* **2003**, *332*, 657−74.
(41) Delarue, M.; Sanejouand, Y.-H. Simplified Normal Mode Analysis of Conformational Transitions in DNA-dependent Polymerases: the Elastic Network Model. *J. Mol. Biol.* **2002**, *320*, 1011−24.

https://doi.org/10.1021/acsomega.4c00523
ACS Omega 2024, 9, 24520−24537

(42) Bakan, A.; Meireles, L. M.; Bahar, I. *ProDy*: Protein Dynamics Inferred from Theory and Experiments. *Bioinformatics.* **2011**, *27*, 1575−7.
(43) Robert, G.; Sollier, A. Equation of state and elastic properties of beryllium from first principles calculations. *Journal de Physique IV (Proceedings)*. **2006**, *134*, 257−62.
(44) Tama, F.; Sanejouand, Y.-H. Conformational change of proteins arising from normal mode calculations. *Protein Engineering, Design and Selection.* **2001**, *14*, 1−6.
(45) Fuglebakk, E.; Tiwari, S. P.; Reuter, N. Comparing the intrinsic dynamics of multiple protein structures using elastic network models. *Biochimica et Biophysica Acta (BBA) - General Subjects.* **2015**, *1850*, 911−22.
(46) Lins, L.; Thomas, A.; Brasseur, R. Analysis of accessible surface of residues in proteins. *Protein Sci.* **2003**, *12*, 1406−17.
(47) Blom, N.; Gammeltoft, S.; Brunak, S. Sequence and structure-based prediction of eukaryotic protein phosphorylation sites. *J. Mol. Biol.* **1999**, *294*, 1351−62.
(48) Pettersen, E. F.; Goddard, T. D.; Huang, C. C.; Couch, G. S.; Greenblatt, D. M.; Meng, E. C.; et al. UCSF Chimera–a visualization system for exploratory research and analysis. *J. Comput. Chem.* **2004**, *25*, 1605−12.
(49) Humphrey, W.; Dalke, A.; Schulten, K. VMD: Visual molecular dynamics. *J. Mol. Graph.* **1996**, *14*, 33−8.

https://doi.org/10.1021/acsomega.4c00523
ACS Omega 2024, 9, 24520−24537